

**NUCLEAR DATA AND MEASUREMENTS SERIES**

**ANL/NDM-20**

**Fast-Neutron Gamma-Ray Production  
from Elemental Iron:  $E_n \leq 2$  MeV**

by

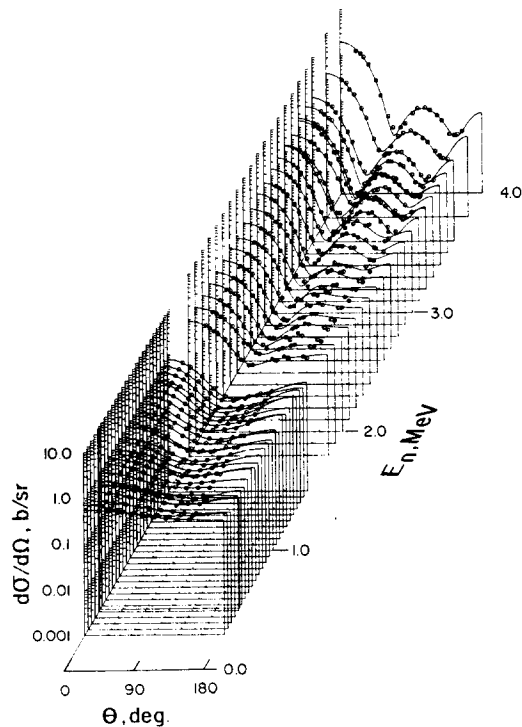
Donald L. Smith

May 1976

**ARGONNE NATIONAL LABORATORY,  
ARGONNE, ILLINOIS 60439, U.S.A.**

# NUCLEAR DATA AND MEASUREMENTS SERIES

ANL/NDM-20  
FAST-NEUTRON GAMMA-  
RAY PRODUCTION FROM  
ELEMENTAL IRON:  
 $E_n \sim 2$  MeV  
by  
Donald L. Smith  
May 1976



ARGONNE NATIONAL LABORATORY,  
ARGONNE, ILLINOIS 60439, U.S.A.

The facilities of Argonne National Laboratory are owned by the United States Government. Under the terms of a contract (W-31-109-Eng-38) between the U. S. Atomic Energy Commission, Argonne Universities Association and The University of Chicago, the University employs the staff and operates the Laboratory in accordance with policies and programs formulated, approved and reviewed by the Association.

#### MEMBERS OF ARGONNE UNIVERSITIES ASSOCIATION

The University of Arizona	Kansas State University	The Ohio State University
Carnegie-Mellon University	The University of Kansas	Ohio University
Case Western Reserve University	Loyola University	The Pennsylvania State University
The University of Chicago	Marquette University	Purdue University
University of Cincinnati	Michigan State University	Saint Louis University
Illinois Institute of Technology	The University of Michigan	Southern Illinois University
University of Illinois	University of Minnesota	The University of Texas at Austin
Indiana University	University of Missouri	Washington University
Iowa State University	Northwestern University	Wayne State University
The University of Iowa	University of Notre Dame	The University of Wisconsin

#### NOTICE

This report was prepared as an account of work sponsored by the United States Government. Neither the United States nor the United States Atomic Energy Commission, nor any of their employees, nor any of their contractors, subcontractors, or their employees, makes any warranty, express or implied, or assumes any legal liability or responsibility for the accuracy, completeness or usefulness of any information, apparatus, product or process disclosed, or represents that its use would not infringe privately-owned rights.

ANL/NDM-20  
FAST-NEUTRON GAMMA-  
RAY PRODUCTION FROM  
ELEMENTAL IRON:  
 $E_n \sim 2 \text{ MeV}$

by

Donald L. Smith  
May 1976

In January 1975, the research and development functions of the former U.S. Atomic Energy Commission were incorporated into those of the U.S. Energy Research and Development Administration.

Applied Physics Division  
Argonne National Laboratory  
9700 South Cass Avenue  
Argonne, Illinois 60439  
U.S.A.

## NUCLEAR DATA AND MEASUREMENTS SERIES

The Nuclear Data and Measurements Series presents results of studies in the field of microscopic nuclear data. The primary objective is the dissemination of information in the comprehensive form required for nuclear technology applications. This Series is devoted to: a) Measured microscopic nuclear parameters, b) Experimental techniques and facilities employed in data measurements, c) The analysis, correlation and interpretation of nuclear data, and d) The evaluation of nuclear data. Contributions to this Series are reviewed to assure technical competence and, unless otherwise stated, the contents can be formally referenced. This Series does not supplant formal journal publication but it does provide the more extensive information required for technological applications (e.g., tabulated numerical data) in a timely manner.

## TABLE OF CONTENTS

	<u>Page</u>
ABSTRACT . . . . .	3
I. INTRODUCTION . . . . .	4
II. EXPERIMENTAL PROCEDURE . . . . .	6
III. DATA PROCESSING . . . . .	8
IV. CORRECTIONS . . . . .	15
V. ERROR ANALYSIS . . . . .	17
VI. RESULTS AND DISCUSSION . . . . .	18
ACKNOWLEDGEMENTS . . . . .	22
APPENDIX A: MODIFICATIONS TO NEUTRON MULTIPLE SCATTERING CORRECTION CODE "GAMSCT" . . . . .	23
REFERENCES . . . . .	35
TABLES . . . . .	37
FIGURES . . . . .	48

FAST-NEUTRON GAMMA-RAY  
PRODUCTION FROM ELEMENTAL

IRON:  $E_n \lesssim 2 \text{ MeV}$

by

Donald L. Smith

Argonne National Laboratory, Argonne, Illinois 60439, U.S.A.

ABSTRACT

A Ge(Li) detector and a fission detector were used to measure elemental differential-cross-section excitation functions for fast-neutron gamma-ray production from iron relative to fast-neutron fission of  $^{235}\text{U}$ . Data were acquired at  $\sim 50$  keV intervals with  $\sim 50$  keV neutron-energy resolution from near threshold to  $\sim 2$  MeV. Angular distributions for the 0.847-MeV gamma ray were measured at 0.93, 0.98, 1.08, 1.18, 1.28, 1.38, 1.59, 1.68, 1.79, 1.85 and 2.03 MeV. Significant fourth-order terms were required for the Legendre polynomial expansions used in fitting several of these angular distributions. This casts doubt on the accuracy of the commonly used approximation that the integrated gamma-ray production cross section is essentially equal to  $4\pi$  times the 55-degree (or 125-degree) differential cross section. The method employed in processing these data is described. Comparison is made between results from the present work and some previously reported data sets. The uncertainties associated with energy scales, neutron-energy resolution and other experimental factors for these various measurements make it difficult to draw conclusions concerning the observed differences in the values reported for these fluctuating cross sections.

\* This work performed under the auspices of the U.S. Energy Research and Development Administration.

## I. INTRODUCTION

Iron is used extensively in structural components and shielding for nuclear reactors since ferrous materials are relatively inexpensive and their properties can be tailored to satisfy many reactor engineering requirements. Information on neutron interaction phenomena for iron is important in the analysis of nuclear reactor kinetics, radiation damage effects and safety. The latter aspect is particularly relevant because the structural integrity of reactors, and the design of effective biological shielding, both depend upon properties of iron.

Requests for cross section data on the interaction of fast neutrons with iron currently specify accuracies in the range 5-10% for the important processes in effect at neutron energies up to 15 MeV [1]. These include total interaction, capture, elastic and inelastic scattering, (n;p), (n; $\alpha$ ), and gamma-ray production processes. A brief survey of the literature reveals that these requests are largely unsatisfied [2].

Measurements have been made on most of these processes at many laboratories. Unfortunately, differences in the reported cross section values are largely unresolved. Recent high-resolution studies, carried out at both monoenergetic and white-source facilities, have shown that the total, elastic and inelastic scattering cross sections for iron exhibit pronounced structure at energies up to several MeV [3-6]. The existence of this structure appears to offer a plausible explanation for the differences in reported cross section sets. Ideally, energy-averaged high-resolution data should agree with the results of broad-resolution measurements. This has generally not turned out to be the case for iron--at least to within the desired accuracy (< 10%).

The neutron-induced prompt gamma-ray production for neutron energies from 0.86 MeV up to several MeV is dominated by the 0.847-MeV gamma ray associated with excitation of the first-excited state in  $^{56}\text{Fe}$  by the  $^{56}\text{Fe}(n,n'\gamma)^{56}\text{Fe}$  reaction. A 1.408-MeV gamma ray

from the  $^{54}\text{Fe}(n,n'\gamma)^{54}\text{Fe}$  reaction is also observed at energies below 2 MeV, but it is of secondary importance because of the low abundance of  $^{54}\text{Fe}$  (5.82%). Gamma-ray production from neutron reactions with  $^{57}\text{Fe}$  and  $^{58}\text{Fe}$  appears to be unimportant owing to low isotopic abundance. Capture gamma rays are important for low-energy neutrons, however this aspect is not considered in the present report.

The integrated cross section for 0.847-MeV gamma ray production nearly equals the integrated inelastic scattering cross section for the 0.847-MeV level in  $^{56}\text{Fe}$  at energies below 2.085 MeV (only one level is excited and internal conversion is negligible). The 0.847-MeV gamma-ray production cross section has been measured with high resolution at white source facilities [4-6]. The results of these various experiments are in fair agreement on the general shape of the excitation function; differences in detail are noticeable in the vicinity of extrema, probably because of energy scale and resolution differences for these measurements. Differences of  $\sim 10\%$  are observed for the energy-averaged cross sections derived from these high-resolution measurements. Quoted errors for these data are  $\sim 15\%$ . Uncertainties in neutron fluence determination and background subtraction appear to be the major sources of experimental uncertainty for these white-source experiments.

Geometric limitations hamper the measurement of angular distributions at white-source facilities. Gamma-ray production measurements at these facilities have usually been limited to 55 or 125 degrees where nodes exist for the second-order terms of Legendre-polynomial representations of the angular distribution functions. The assumption is made that the fourth-order terms are insignificant. Angular distribution measurements for both inelastic scattering and inelastic gamma-ray production have been made with coarse resolution at various laboratories [2,7]. There are wide differences in the cross sections derived from these measurements. The 0.847-MeV gamma-ray angular distribution

has been observed to be strongly anisotropic near threshold [8], and there is evidence that the inelastic neutron scattering distribution for the 0.847-MeV level in  $^{56}\text{Fe}$  is also somewhat anisotropic and not always symmetric about 90 degrees [3]. Fewer data are available on the cross section for production of the 1.408-MeV gamma ray because the yield is low and less emphasis has been placed on this process [2,7].

The present work was undertaken with the objective of improving the knowledge of the energy-averaged inelastic gamma-ray production cross sections for natural iron near threshold. Emphasis has been placed on measurement (wherever practical) of gamma-ray angular distributions and investigation of the effect of observed anisotropies on the integrated cross sections.

An experimental facility, which was recently developed at the Argonne Fast-Neutron Generator Laboratory, was utilized in the present work [9]. Since the experimental apparatus and details of the measurements are described in an earlier report [9], this topic is covered briefly in Section II. Data processing details, including formulas used in the differential-cross-section calculations, are discussed in Section III (exclusive of the sample absorption and multiple scattering effects which are discussed in Ref. 10 and Appendix A of the present report). Corrections to the data are reviewed in Section IV. An analysis of experimental errors is given in Section V. Finally, the results of the present work, and a comparison with some other reported data, appear in Section VI.

## II. EXPERIMENTAL PROCEDURE

The neutron source for the present measurements was the  $^7\text{Li}(p,n)^7\text{Be}$  reaction. The characteristic neutron spectrum for this source is described in an earlier report [11]. Pulsed and bunched proton beams were obtained from the Argonne National Laboratory Fast-Neutron Generator. Average beam intensities of  $\sim 5 \mu\text{A}$  on target were obtained with a pulse rate of

$\sim 2$  MHz and time resolution of  $\sim 1$  nanosecond. Neutron-energy resolution was primarily dependent upon the thickness of the natural lithium metal deposits which were evaporated onto tantalum backings and used as targets.

Chemically pure ( $> 99\%$ ) natural iron samples, in the form of solid cylinders, were placed on the beam line  $\sim 12$  cm from the neutron source. Two samples were used in the present work. The larger sample had a mass of 337.5 grams and was 3.8 cm high and 3.8 cm in diameter. The smaller sample had a mass of 52.72 grams and was 2 cm high and 2 cm in diameter.

The neutron fluence was measured with a fission detector which contained a 2.54-cm diameter deposit of  $\sim 0.4$  mg of uranium. The isotopic composition of this deposit is:  $^{234}\text{U}$  (0.9%),  $^{235}\text{U}$  (93.3%),  $^{236}\text{U}$  (0.3%) and  $^{238}\text{U}$  (5.5%). Procedures for calibration of this deposit have been reported [12,13]. The fission detector was placed on the beam line between the neutron source and the sample. The distances from the neutron source to the uranium deposit were in the range 5-7 cm. Since calibration of the apparatus was sensitive to the distances from the neutron source to the sample and to the fission detector, these distances were measured with a micrometer and were rechecked periodically during the experiment.

The gamma radiation produced by fast-neutron bombardment of the iron samples was measured with a 52-cm<sup>3</sup> true-coaxial Ge(Li) detector. This detector was placed in a shield which pivots around the sample position through the angular range 30 - 135 degrees. The relative full-energy peak efficiency for this detector was measured using a series of radioactive gamma-ray sources, including  $^{56}\text{Co}$ ,  $^{60}\text{Co}$ ,  $^{22}\text{Na}$ ,  $^{152}\text{Eu}$ ,  $^{133}\text{Ba}$ , etc., over the range  $E_{\gamma} = 0.1-3.5$  MeV [9]. The absolute efficiency was measured at 0.662, 1.274 and 1.333 MeV using U.S. National Bureau of Standards calibrated  $^{137}\text{Cs}$ ,  $^{22}\text{Na}$  and  $^{60}\text{Co}$  sources placed at the sample position.

A current integrator and plastic scintillator were used as secondary monitors for relative measurements. Excitation

functions near 55 and 90 degrees were measured with the fission detector in place. Angular distribution measurements were made with the fission detector removed from its normal position; the integrator and plastic scintillator were then used as the monitors.

Time-of-flight techniques were used to reduce background and the experimental data were recorded with an on-line computer system [9,14]. Gamma-ray pulse-height spectra, time-of-flight spectra for the gamma-ray detector, fission detector and scintillation detector, as well as integrator and long counter counts were stored in the computer.

Most of the measurements were performed using the 337.5-gram iron sample in order to enhance the data accumulation rate. The corrections for absorption and scattering in this sample were large. These corrections affected the absolute normalization of the measured cross sections significantly, but had much less influence on the shapes of the excitation functions and angular distributions. Measurements were therefore made at several energies using the 52.72-gram sample. Since the corrections for this sample were considerably smaller, these data were then utilized to establish the absolute cross section normalization for the entire experiment.

Specific sets of large-sample data acquired in the present experiment were:

- i) yield of the 0.847-MeV gamma ray near 90 degrees, with  $\sim$  45 keV resolution and energy steps of  $\sim$  50 keV, from 0.9 to 1.32 MeV,
- ii) yield of the 0.847-MeV gamma ray near 55 degrees, with  $\sim$  65 keV resolution and energy steps of  $\sim$  50 keV, from 0.89 to 2.04 MeV,
- iii) angular distributions of the 0.847-MeV gamma ray with  $\sim$  65 keV resolution at neutron energies of 0.93, 0.98, 1.08, 1.18, 1.28, 1.38, 1.59, 1.68, 1.79, 1.85 and 2.03 MeV,
- iv) yield of the 1.408-MeV gamma ray near 55 degrees, with  $\sim$  65 keV resolution and energy steps of  $\sim$  50 keV, from 1.5 to 2.04 MeV.

### III. DATA PROCESSING

The counts in the 0.847- and 1.408-MeV gamma-ray full-energy peaks were obtained after subtraction of background. The monitor

counts were obtained from the appropriate peak in the time-of-flight spectra whenever the fission detector (or scintillation detector) served as the monitor.

The computation of cross sections from the measured quantities is complicated because of numerous experimental details which must be considered. These include geometry, secondary neutron groups from the source reaction, lithium target thickness, and the absorption and multiple scattering of neutrons and gamma rays. The formalism for these computations is outlined below for the case where the fission detector serves as the monitor. Analysis of data acquired using the integrator or plastic scintillator as a monitor is simpler since the monitor counts require no corrections.

In performing the cross-section calculations, the lithium target is divided into  $n_T$  layers ( $i_T = 1, \dots, n_T$ ), the uranium deposit is divided into  $n_F$  concentric annuluses ( $i_F = 1, \dots, n_F$ ) and the sample is divided into  $n_S$  volume elements (defined in Ref. 10) designated here by the index  $j$  ( $j = 1, \dots, n_S$ ). The four uranium isotopes found in the uranium deposit are designated by the index  $l$  ( $l = 1, \dots, 4$ ). The neutron spectrum from the lithium target has two discrete groups and an additional low-energy continuum group. The continuum group is represented by several (usually 10) adjacent discrete groups for computational purposes. The total number of neutron groups is designated  $n_G$  ( $i_G = 1, \dots, n_G$ ).

The relationship between the observed fission detector counts and the fission cross sections for the uranium isotopes in the deposit is given by the formula

$$Y_F = \left( \frac{2 C_{FH}}{n_F R_F} \right) \sum_{i_T}^{n_T} \sum_{i_G}^{n_G} C_{FN} C_{FP} \sum_{i_F}^{n_F} F d_{Fi_F}^{-2} r_{Fi_F} \left( \sum_{l=1}^4 N_{Ul} \sigma_{Fl} \right) \quad (1)$$

where

$Y_F$  = observed fission detector counts,

- $C_{FH}$  = a constant correction factor,  
 $R_F$  = radius of uranium deposit,  
 $C_{FN}$  = correction dependent upon neutron energy,  
 $C_{FP}$  = correction dependent upon proton energy,  
 $F$  = neutron fluence (neutrons/sr),  
 $d_{Fi_F}$  = distance from neutron source to the annulus,  
 $r_{Fi_F}$  = mean radius of the annulus,  
 $N_{U\ell}$  = absolute number of atoms of  $\ell$ -th isotope in the uranium deposit,  
 $\sigma_{F\ell}$  = fission cross section for  $\ell$ -th isotope of the uranium sample at the appropriate energy.

The expressions utilized for calculating the neutron fluence  $F$  were obtained from Appendix A of Ref. 11. The overall normalization of  $F$  is unimportant since ratio measurements were made in the present experiment.

The relationship between the observed gamma-ray detector counts and the gamma-ray production differential cross section is given by the formula

$$Y_S = C_{SH} D_\gamma^2 \left( \frac{N_S}{V_S} \right) g (\Omega_{DET} \epsilon_{DET}) \sum_{i_T}^{n_T} \sum_{i_G}^{n_G} C_{SN} C_{SP} C_{SS} \cdot \sum_j^{n_S} F d_{nj}^{-2} \eta_{nj} v_j \left( \frac{d\sigma}{d\Omega} \right) \eta_{\gamma j} d_{\gamma j}^{-2} \quad (2)$$

where

- $Y_S$  = observed gamma-ray detector full-energy peak counts,  
 $C_{SH}$  = a constant correction factor,  
 $D_\gamma$  = distance from the center of the sample to the gamma-ray detector,  
 $N_S$  = number of atoms in the sample (iron in the present work).

$V_S$  = volume of the sample,

$g$  = a constant geometrical factor

$(\Omega_{DET} \epsilon_{DET})$  = effective efficiency of the gamma-ray detector  
for the gamma-rays under consideration,

$C_{SN}$  = correction dependent upon neutron energy,

$C_{SP}$  = correction dependent upon proton energy,

$C_{SS}$  = correction for neutron multiple scattering in the  
sample,

$F$  = neutron fluence (see discussion above),

$d_{nj}$  = distance from neutron source to the  $j$ th element of  
the sample,

$\eta_{nj}$  = neutron absorption factor ( $\eta_n = e^{-\Sigma_{nT} \delta_n}$ ),

$\Sigma_{nT}$  = neutron macroscopic total cross section,

$\delta_n$  = neutron path length in the sample,

$v_j$  = a variable geometrical factor,

$\left(\frac{d\sigma}{d\Omega}\right)$  = microscopic gamma-ray production differential cross  
section for the process under consideration,

$\eta_{\gamma j}$  = gamma-ray absorption factor ( $\eta_\gamma = e^{-\Sigma_{\gamma T} \delta_\gamma}$ ),

$\Sigma_{\gamma T}$  = gamma-ray macroscopic total cross section,

$\delta_\gamma$  = gamma-ray path length in the sample,

$d_{\gamma j}$  = distance from  $j$ th element of the sample to the gamma-  
ray detector.

The expression on the right-hand side of Eq. (1) can be computed directly since all the quantities in it, including the fission cross sections for the monitor, are presumed to be known.

The right-hand side of Eq. (2) contains the differential cross section,  $\left(\frac{d\sigma}{d\Omega}\right)$ , which is presumed to be unknown and actually is the

quantity sought from the measurements. Furthermore, values of this differential cross section at various energies and angles are needed for the computation. Clearly, an approximation is required in order to proceed with the analysis.

The procedure used in the present work is given below. Define

$\langle E_n \rangle$  = average first-group neutron energy,

$\langle \theta_{n\gamma} \rangle$  = average scattering angle for the measurement,

$\left( \frac{d\sigma}{d\Omega} \right)_{\text{approx}}$  = an approximation to the true gamma-ray production differential cross section.

In the present work,  $\left( \frac{d\sigma}{d\Omega} \right)_{\text{approx}}$  was derived from the ENDF/B-IV file for natural iron [15].

Let

$$\delta_{i_T i_G j} = C_{SN} C_{SP} C_{SS} F_{d_{nj}}^{-2} n_{nj} v_j \left( \frac{d\sigma}{d\Omega} \right)_{\text{approx}} n_{\gamma j} d_{\gamma j}^{-2}, \quad (3)$$

then

$$\langle E_n \rangle \equiv \frac{\sum_{i_T}^{n_T} \sum_j^{n_S} E_n \delta_{i_T 1 j}}{\sum_{i_T}^{n_T} \sum_j^{n_S} \delta_{i_T 1 j}}, \quad (4)$$

$$\langle \theta_{n\gamma} \rangle \equiv \frac{\sum_{i_T}^{n_T} \sum_j^{n_S} \theta_{n\gamma} \delta_{i_T 1 j}}{\sum_{i_T}^{n_T} \sum_j^{n_S} \delta_{i_T 1 j}}. \quad (5)$$

If

$\left\langle \left( \frac{d\sigma}{d\Omega} \right) \right\rangle$  = true gamma-ray production differential cross section corresponding to energy  $\langle E_n \rangle$  and scattering angle  $\langle \theta_{n\gamma} \rangle$ ,

$\langle \left( \frac{d\sigma}{d\Omega} \right) \text{approx} \rangle =$  approximate gamma production differential cross section for energy  $\langle E_n \rangle$  and scattering angle  $\langle \theta_{n\gamma} \rangle$ ,

and

$$\mathcal{I}_{i_T i_G j} = \mathcal{I}_{i_T i_G j} / \langle \left( \frac{d\sigma}{d\Omega} \right) \text{approx} \rangle, \quad (6)$$

then

$$Y_S \approx C_{SH} D_Y^2 \frac{N_S}{V_S} g(\Omega_{DET} \epsilon_{DET}) \langle \left( \frac{d\sigma}{d\Omega} \right) \rangle. \quad (7)$$

$$\sum_{i_T}^{n_T} \sum_{i_G}^{n_G} \sum_j^{n_S} \mathcal{I}_{i_T i_G j}.$$

It is clear from Eqs. (2)-(7) that the approximation involves the use of the approximate cross section  $\left( \frac{d\sigma}{d\Omega} \right) \text{approx}$  to represent the true cross section  $\left( \frac{d\sigma}{d\Omega} \right)$  in the computation of the cross section ratio  $\xi_\gamma$ ,

$$\xi_\gamma = \left\{ \left( \frac{d\sigma}{d\Omega} \right) / \langle \left( \frac{d\sigma}{d\Omega} \right) \rangle \right\} \approx \left\{ \left( \frac{d\sigma}{d\Omega} \right) \text{approx} / \langle \left( \frac{d\sigma}{d\Omega} \right) \text{approx} \rangle \right\} \quad (8)$$

This proves to be a reasonable approximation since the ratio  $\xi_\gamma$  is found to be rather insensitive to the details of the differential cross section when smooth cross sections or energy-averaged cross sections are involved.

Let

$$\mathcal{F}_{i_T i_G i_F} = C_{FN} C_{FP}^F d_{Fi_F}^{-2} r_{Fi_F} \left( \sum_{\ell}^4 N_{U\ell} \sigma_{F\ell} \right), \quad (9)$$

then Eq. (1) can be written as

$$Y_F = \left( \frac{2 C_{FH}}{n_F R_F} \right) \sum_{i_T}^{n_T} \sum_{i_G}^{n_G} \sum_{i_F}^{n_F} \mathcal{F}_{i_T i_G i_F}. \quad (10)$$

Then, from Eqs. (7) and (10)

$$\left\langle \frac{d\sigma}{d\Omega} \right\rangle \approx \left( \frac{Y_S}{Y_F} \right) \cdot \frac{\left( \frac{2C_{FH}}{n_F R_F} \right) \sum_{i_T}^{n_T} \sum_{i_G}^{n_G} \sum_{i_F}^{n_F} \mathcal{F}_{i_T i_G i_F}}{C_{SH}^D \gamma^2 \left( \frac{N_S}{V_S} \right) g (\Omega_{DET} \epsilon_{DET}) \sum_{i_T}^{n_T} \sum_{i_G}^{n_G} \sum_j^{n_S} \mathcal{J}_{i_T i_G j}} \quad (11)$$

Eq. (11) relates the gamma-ray production differential cross section  $\left\langle \frac{d\sigma}{d\Omega} \right\rangle$  for energy  $\langle E_n \rangle$  and angle  $\langle \Theta_{n\gamma} \rangle$  to the measured detector counts  $Y_S$  and  $Y_F$ .

Neutron absorption and scattering cross sections required for the analysis were obtained from the ENDF/B-IV file for iron [15]. These cross sections were smoothed to a resolution consistent with the present experiment. Photon absorption cross sections were obtained from an evaluation by Storm and Israel [16].

The differential gamma-ray production cross section can be expressed by the formula

$$\left( \frac{d\sigma}{d\Omega} \right) = \frac{\sigma}{4\pi} [ 1 + \omega_2 P_2(\cos \Theta) + \omega_4 P_4(\cos \Theta) ] \quad (12)$$

where  $\sigma$  is the integrated cross section. This formula applies for both the 0.847- and 1.408-MeV gamma rays since each corresponds to an E2 transition between a  $2^+$  excited state and a  $0^+$  ground state. Also, gamma-ray production is symmetric around 90 degrees.

Angular distribution data were fitted by least squares with this Legendre polynomial expansion and  $\omega$  coefficients were deduced from the analysis. These  $\omega$  coefficients, and measured differential cross sections, were used to calculate integrated cross section values. This procedure proved worthwhile only for the 0.847-MeV gamma-ray data since the uncertainties in the angular distribution data for the 1.408-MeV gamma ray were large. The integrated cross sections for production of the 1.408-MeV gamma ray are approximated by  $4\pi$  times the 55-degree differential cross sections in the present work.

#### IV. CORRECTIONS

Several corrections to the experimental data are combined into the factors  $C_{FH}$ ,  $C_{FN}$ ,  $C_{FP}$ ,  $C_{SH}$ ,  $C_{SP}$  and  $C_{SS}$  which appear in the formulas of Section III. Some corrections were computed while others were measured. Several other effects were investigated and found to be insignificant.

The scintillation detector and integrator were used as monitors only for relative measurements; uncorrected monitor counts were found to be adequate for these applications. The fission detector was used in absolute cross section measurements, and several corrections were applied to the observed fission counts.

Two effects led to a reduction of counts in the fission detector. One was the loss of fission fragments emitted near 90 degrees, because of the finite thickness of the uranium deposit; the second was the rejection of low-energy fragment pulses, along with unwanted alpha-particle pulses, by a discriminator. The combined correction was  $\sim 3.8\%$  for all energies and was included in the factor  $C_{FH}$  [12].

Room-return neutrons produced a random background of  $\sim 2\%$  in the fission detector TOF spectrum. This background was automatically rejected since only the counts under the TOF peaks produced by prompt neutrons were considered in the data processing.

Neutron scattering by components of the fission detector necessitated a neutron-energy dependent correction to the observed fissions. This correction was calculated and it was found that "In" scattering exceeded "Out" scattering. The net correction was only  $\sim 1-2\%$  owing to the low-mass construction of the fission detector used in this work. The backscattering of neutrons from the sample produced a correction of  $< 1\%$  for the 337.5-gram iron sample. Since this correction was too small to be measured reliably, it was calculated. These two neutron-energy dependent corrections were included in the factor  $C_{FN}$ . There were no significant proton-energy dependent corrections, so  $C_{FP}$  was assumed to be unity in all computations.

The presence of the fission detector between the neutron source and the sample affected the neutron fluence at the sample. The

correction for this effect was dependent upon neutron energy, and it was found that "Out" scattering dominated "In" scattering thereby producing a net reduction of neutron fluence. The correction was  $\sim 1-1.5\%$  and it appears in  $C_{SN}$ . It was also calculated.

Neutrons incident upon the fission detector produced gamma rays from  $Fe(n,n'\gamma)$  reactions with the detector walls. A correction for this effect was measured by using samples of vanadium and nickel in place of the large iron sample. The correction amounted to about 10% well above threshold. The problem did not arise in measurements with the small sample because small sample cross sections were measured relative to large sample cross sections using the secondary monitors. The fission detector was removed during these ratio measurements and no background  $Fe(n,n'\gamma)$  lines were observed under these conditions.

Corrections for multiple scattering were computed using code GAMSCT described in Ref. 10 and in Appendix A of the present report. This correction appears in  $C_{SS}$  and amounted to about 10-20% for the small sample and 20-40% for the large sample at energies well above threshold.

Several corrections which were investigated produced negligible effects on the final results. These were:

- i) neutron scattering by the target backing ( $< 0.1\%$ ),
- ii) neutron scattering by the gamma-detector shield ( $< 0.5\%$ ),
- iii) finite beam spot ( $< 0.1\%$ ),
- iv) air scattering ( $< 0.2\%$ ),
- v) coherent scattering of gamma rays by the sample ( $\sim 0.1\%$ ),
- vi) neutrons from tantalum target backing (no effects observed),
- vii) neutron scattering by fission chamber support structure ( $< 0.2\%$ ).

viii) gamma rays from iron used in gamma-ray detector shield (no effects observed).

The small sample cross sections were found to be systematically larger than the corresponding large sample cross sections by a factor of  $\sim 6\%$ . This difference was attributed to a systematic error in computation of the neutron and gamma-ray transmission factors. These factors were computed utilizing published cross sections [15,16] which are subject to uncertainty. It is also possible that fluctuation effects in the neutron total cross section could produce a noticeable systematic error in computation of energy-averaged neutron transmission factors for the large sample [17]. Since the transmission factors for the small sample are much closer to unity than for the large sample, the effect of these uncertainties on the measured small sample cross sections is probably not significant within the accuracy of the present experiment. It is believed that the small sample cross sections more nearly resemble the microscopic cross sections. Therefore, all the large sample cross sections were renormalized upward by 6% for consistency in this experiment.

## V. ERROR ANALYSIS

The calculations described in the present report and in Ref. 10 were performed with a digital computer. Therefore, it was relatively simple to test the sensitivity of the computed quantities to all the parameters used in the calculations. Estimates were made of the uncertainties in these parameters and the effect of these uncertainties on the final results were determined for the large sample measurements. The results are summarized in Table I. The overall uncertainties are root-mean-square composites of partial errors listed in this table.

The total error is  $\pm 11\%$  for the ratio of the 0.847-MeV gamma-ray production differential cross section to the effective fission cross section for the uranium deposit, and  $\pm 14\%$  for the corresponding error for the 1.408-MeV gamma ray. The cross section for  $^{235}\text{U}$  fission, the dominant process in the present

experiment, has achieved the status of a standard in recent years and is probably known to within  $\pm 5\%$  for the energy range in question. When this error is combined with the error in the measured ratios, an overall root-mean-square error of  $\pm 12\%$  is deduced for the absolute differential cross sections for production of the 0.847-MeV gamma ray. The corresponding error for the 1.408-MeV gamma ray is  $\pm 15\%$ .

## VI. RESULTS AND DISCUSSION

The data obtained for the 0.847-MeV gamma ray are more extensive than for the 1.408-MeV gamma ray; the former will be discussed first. All the iron cross sections appearing in the present report are elemental rather than isotopic.

### 0.847-MeV Gamma Ray

The measured cross section ratios and the resultant gamma-ray production differential cross sections, computed using ENDF/B-IV [15] fission cross sections, are presented in Table II. In accordance with the discussion in Section V, the overall error for the cross section ratios is  $\pm 11\%$  and for the computed differential cross sections it is  $\pm 12\%$ . Fig. 1 is a plot of  $4\pi$  times the measured differential cross sections near 55 degrees. Also shown is the corresponding ENDF/B-IV [15] evaluation of the inelastic scattering cross section for the first-excited state in  $^{56}\text{Fe}$ . The evaluated data were smoothed to 50 keV resolution before plotting as indicated in Fig. 2. The evaluated curve agrees well with the results from the present work.

The measured angular distributions are expressed in the dimensionless form  $[W(\theta)/W(90^\circ)]$  in Table III and Fig. 3. The errors of  $\pm 5\%$  represent only the uncertainty in determination of the gamma ray counts. The measured angular distributions can be fitted quite nicely by Legendre polynomial expansions containing only even-order terms (symmetric about 90 degrees). The need for

a  $P_4$  term is evident from the shape of the distributions at forward and backward angles. The  $\omega$  coefficients derived from the fitting procedure are presented in Table IV. The assigned errors are standard deviations computed as by products of the fitting procedure. An attempt was made to fit the angular distributions without a  $P_4$  term. These fits were generally poor and yielded relatively large standard deviations. The derived values for  $\omega_4$  are negative at most energies. This leads to integrated cross sections which are generally smaller than  $4\pi$  times the differential cross sections at 55 degrees.

The differential cross section and angular distribution data from Tables II-IV were used, in conjunction with Eq. (12), to compute integrated cross sections. Table IV was interpolated linearly to obtain values of  $\omega_2$  and  $\omega_4$  for intermediate energies. Ratios of the resultant integrated cross sections to  $4\pi$  times the differential cross sections at 55 degrees were also computed using the same formula and data. These derived quantities are presented in Table V, and the integrated cross sections are plotted in Fig. 4 along with the smoothed ENDF/B-IV [15] evaluation.

It is clear from Table V that  $4\pi$  times the 55-degree differential cross section is not a particularly good approximation to the integrated cross section in this threshold region. Below 1 MeV, the  $P_4$  term contributes 10% or more to the integrated cross section. The integrated cross sections derived from data measured near 55 degrees and 90 degrees are in reasonable agreement (see Fig. 4). These two data sets were measured during separate periods almost a year apart.

Integrated gamma-ray production cross sections for the 0.847-MeV gamma ray, derived from the present work, are lower than the values from the ENDF/B-IV [15] evaluation owing to angular distribution effects. This is understandable since the ENDF/B-IV [15] evaluation appears to be based upon high resolution data acquired from a white-source experiment in which measurements were performed at a  $P_2$  node. The disagreement cannot be considered a discrepancy

because, in fact, two different quantities are being compared.

A detailed review of the extensive literature [2] on this subject is beyond the scope of the present work. Some of the reported data are available from the CSISRS file at the National Neutron Cross Section Center [7] and were therefore readily obtained for comparison with results from the present work. The contents of this file are summarized in Fig. 5. The smoothed ENDF/B-IV evaluation is also shown. Adjustments were made to several of the data sets from the CSISRS file [7], prior to inclusion in the plot, so that comparison with the present results would be more meaningful. Isotopic cross sections were converted to elemental values. High-resolution results were averaged to  $\sim 50$  keV resolution. When integrated cross sections were not reported,  $4\pi$  times the 55-degree differential cross sections were plotted (for both inelastic neutron and gamma-ray data). No distinction was made between  $(n,n')$  and  $(n,n'\gamma)$  data since the integrated cross sections should be nearly identical at these low energies. Credits to the authors appear in the legend of Fig. 5. The reader can refer to the CSISRS file [7] for references and additional experimental details.

There are significant differences in the data sets plotted in Fig. 5. The ENDF/B-IV [15] evaluation is based on recent high resolution data. The results of the present experiment tend to confirm this evaluation insofar as 55-degree data is concerned. The ENDF/B-IV [15] evaluation overestimates the integrated cross section because it is based upon data which does not take detailed angular distribution effects into consideration. While there are several data sets in Fig. 5 which agree with the results of the present work, as presented in Fig. 4, many of these are based on single-angle measurements so that comparison is not very meaningful.

Smith [17] recently conducted a neutron scattering experiment at Argonne National Laboratory in which the inelastic scattering ( $Q = -0.847$  MeV) cross section for iron was measured in the

range 1.6-2.0 MeV. Since angular distributions were obtained, the results of these measurements can be readily compared with the present work. Values of the integrated cross section obtained by Smith [17] are plotted in Fig. 4. The agreement with the present results is satisfactory.

#### 1.408-MeV Gamma Ray

The measured cross section ratios near 55 degrees, and the resultant gamma-ray production differential cross sections computed using ENDF/B-IV [15] fission cross sections, are presented in Table VI. Since no angular distribution data were obtained for this gamma ray, the integrated cross sections have been approximated by  $4\pi$  times the measured differential cross sections. These integrated cross sections are listed in Table VI and are plotted in Fig. 6 along with the ENDF/B-IV [15] evaluation for this reaction. As discussed in Section V, the overall error for the ratios is  $\pm 14\%$  and for the cross sections is  $\pm 15\%$ .

The data available from the literature for comparison with the present results is limited. The contents of the CSISRS file [7] from the National Neutron Cross Section Center have been plotted in Fig. 7. These data were adjusted, where necessary, as discussed above for the 0.847-MeV gamma ray. The available experimental data do not define the cross section well since large differences exist in the reported values. The ENDF/B-IV [15] evaluation appears to be the result of a model calculation. This evaluation is in fair agreement with the results from the present experiment. The evaluation neglects fluctuations seen in the experimental results, and the evaluated cross sections appear too large in the range 1.6-1.8 MeV. The existence of fluctuations in the excitation function is not surprising in view of the fact that the nuclei  $^{54}\text{Fe}$  and  $^{56}\text{Fe}$  differ by only two neutrons and should be structurally similar.

## ACKNOWLEDGEMENTS

The calibrated uranium deposit used in this experiment was obtained from J. W. Meadows. The author is indebted to A. B. Smith for permission to quote unpublished results from his recent measurements.

## APPENDIX A

### MODIFICATIONS TO NEUTRON MULTIPLE SCATTERING CORRECTION CODE "GAMSCT"

The computer code GAMSCT, which is used for computation of corrections for neutron multiple scattering in solid-cylinder samples, has been modified. One modification allows computations to be made using a finite resolution for the neutron-producing reaction. Another modification corrects an error in the procedure used for coordinate transformations. This error appears to have little effect on the computed results.

The original version of GAMSCT (Ref. 10) assumed that a monoenergetic beam of particles with energy  $E_t$  impinges upon an infinitesimally thin target to produce neutrons whose energies are essentially monoenergetic except for kinematic broadening. In reality,  $E_t$  varies within a range ( $E_{t,\min}$ ,  $E_{t,\max}$ ) because of unavoidable spread due to beam-energy resolution and target thickness effects. The modified version of GAMSCT selects  $E_t$  at random in this range according to the formula

$$E_t = E_{t,\min} + R(E_{t,\max} - E_{t,\min}) \quad (13)$$

where  $R$  is a random number from the interval (0,1). Any value of  $E_t$  in the range ( $E_{t,\min}$ ,  $E_{t,\max}$ ) is assumed to be equally probable which implies a "square" resolution function. This assumption is an approximation which appears adequate for most applications. The effects of resolution are found to be relatively unimportant except near the reaction threshold.

Eqs.(64)-(65) from Ref.10 have been found to be in error as they neglect the effects of coordinate-system rotations which must be considered following the scattering of neutrons. The problem is most easily formulated in terms of direction cosines. The method is described in Chapter VII of Ref.18 and will not be reproduced in this report. The consequences of this error are minimal. The modified version of GAMSCT corrects this error.

A listing of the modified version of GAMSCT follows. The dimensions of several arrays have been enlarged because the memory capacity of the computer used for these calculations was increased by the addition of a memory module after Ref. 10 was issued.

GAMSCT=D.L.SMITH-SEL 840MP

DIMENSION ENT(350),SIGNT(350),EGP(350),SIGGP(350),NWGP(6),EWGP(6,3  
10),WGP(6,30),QNS(6),A2NS(6),NNS(6),ENS(6,350),SIGNS(6,350),MWNS(6)  
2,NWNS(6,10),EWNS(6,10,30),WNS(6,10,30),DSIGNS(6),WT(10),YLD(5),YLD  
3SUM(5),PSI(6),INDEX(4),JINDEX(5),NHIT(5),NLEV(6),A(350),B(350),WORK  
4(350)

DATA PI/3,14159/

VALUE(V,VMIN,VMAX)=VMIN+V\*(VMAX-VMIN)  
SEPAR(X1,Y1,Z1,X2,Y2,Z2)=SQRT((X1-X2)\*(X1-X2)+(Y1-Y2)\*(Y1-Y2)+(Z1-  
1Z2)\*(Z1-Z2))

CONTROL

TRACE 813

1 READ(4,2) IC

2 FORMAT(I1)

GO TO(10,20,30,50),IC

10 PAUSE

GO TO 1

READ INTERPOLATION TABLES

20 READ(4,21) MNT

21 FORMAT(16I5)

READ(4,22) (ENT(I),SIGNT(I),I=1,MNT)

22 FORMAT(8E10,4)

READ(4,21) MGP

READ(4,22) (EGP(I),SIGGP(I),I=1,MGP)

READ(4,21) MWGP

IF(MWGP) 23,25,23

23 DO 24 I=1,MWGP

READ(4,21) NWGP(I)

M=NWGP(I)

24 READ(4,22) (EWGP(I,J),WGP(I,J),J=1,M)

25 READ(4,21) MNS

DO 28 I=1,MNS

READ(4,22) QNS(I),A2NS(I)

READ(4,21) NNS(I)

M=NNS(I)

READ(4,22) (ENS(I,J),SIGNS(I,J),J=1,M)

READ(4,21) MWNS(I)

IF(MWNS(I)) 26,28,26

26 L=MWNS(I)

DO 27 J=1,L

READ(4,21) NWNS(I,J)

M=NWNS(I,J)

27 READ(4,22) (EWNS(I,J,K),WNS(I,J,K),K=1,M)

28 CONTINUE

READ AND WRITE BASIC PARAMETERS

30 READ(4,31) NSCAT,NHIST

31 FORMAT(I1,I6)

READ(4,22) RS,M,DNO,DGO

READ(4,22) EG,SIGGT,ENTHG

READ(4,22) A1T,A2T,QT

```

READ(4,32) ETAV,DET,NWT
32 FØRMAT(2E10,4,15)
   IF(NWT) 34,34,33
33 READ(4,22) (WT(I),I=1,NWT)
34 WRITE(5,35) NSCAT,NHIST
35 FØRMAT(1H1/11HNSCAT,NHIST/12,16)
   WRITE(5,36) RS,H,DNO,DGO
36 FØRMAT(12HRS,H,DNO,DGO/4E10,4)
   WRITE(5,37) EG,SIGGT,ENTHG
37 FØRMAT(14HEG,SIGGT,ENTHG/3E10,4)
   WRITE(5,38) A1T,A2T,QT
38 FØRMAT(10HA1T,A2T,QT/3E10,4)
   WRITE(5,39) ETAV,DET,NWT
39 FØRMAT(12HETAV,DET,NWT/2E10,4,15)
   IF(NWT) 40,42,40
40 WRITE(5,41)
41 FØRMAT(5HWT(I))
   WRITE(5,22) (WT(I),I=1,NWT)
42 WRITE(5,43)
43 FØRMAT(/5H,,,,)

```

C  
C  
C

READ AND WRITE SCATTERING ANGLE, CONVERT TO RADIANS

```

50 READ(4,22) THTANK
   WRITE(5,51) THTANK
51 FØRMAT(/7HTHTANK=,E10,4)
   THDET=F1*THTANK/180.0

```

C  
C  
C

PRELIMINARY CALCULATIONS

```

   IF(DET) 53,53,52
52 ETMIN=ETAV-0,5*DET
   ETMAX=ETAV+0,5*DET
53 CONTINUE
   RSRS=RS*RS
   HH=H*H
   HD2=0,5*H
   R1MIN=LNO-RS
   R1MAX=SQRT(DNO*LNO+2,0*DNO*RS+2,0*RSRS+0,25*HH)
   TH1MAX=ATAN(SQRT(0,25*HH+RSRS)/R1MIN)
   VOL1=2,0*PI*(R1MAX-R1MIN)*TH1MAX
   RMAX=SQRT(HH+8,0*RSRS)
   VOLH=2,0*PI*PI*RMAX
   YD=DGO*SIN(THDET)
   ZD=DNO+LGO*COS(THDET)
   DØ 60 J=1,NSCAT
   NHIT(I)=0
60 YLDSUM(I)=0,0
   DØ 61 J=1,MNS
61 NLEV(I)=0
   IHIST=1

```

C  
C  
C  
C  
C  
C  
C

.....START OF HISTORY LOOP

CALCULATE INCIDENT ENERGY. ET=ETAV IF DET=0. IF DET.GT.0,  
DEDUCE ET BY RANDOM SELECTION IN RANGE DET CENTERED ABOUT  
ETAV

```

100 CONTINUE
   IF(DET) 101,101,102

```

```

101 ET=ETAV
    G0 T0 103
102 R=RANF(-1)
    ET=VALUE(R,ETMIN,ETMAX)
103 CONTINUE

    D0 104 I=1,NSCAT
104 JNDEX(I)=0

    SELECT SCATTERING POINT S(1)

    R=RANF(-1)
    RR=VALUE(R,R1MIN,R1MAX)
    R=RANF(-1)
    TH=VALUE(R,0,0,TH1MAX)
    R=RANF(-1)
    PHI=VALUE(R,-PI,PI)
    SINTH=SIN(TH)
    U=SINTH*COS(PHI)
    V=SINTH*SIN(PHI)
    W=COS(TH)
    X=RR*U
    Y=RR*V
    Z=RR*W
    IF(X+HD2) 700,700,150
150 IF(X-HD2) 151,700,700
151 ZMDNO=Z-DNO
    TEST=Y*Y+ZMDNO*ZMDNO
    IF(TEST-RSRS) 152,700,700
152 JNDEX(1)=1
    NHIT(1)=NHIT(1)+1
    CALL ANGLE(X,Y,Z,0.0,0.0,0.0,0.0,0.0,0.0,DNO,0.0,0.0,0.0,0.0,THT)

    CALCULATE NEUTRON ENERGY AND FLUX AT POINT S(1)

    CALL KINAM(A1T,A2T,1.0087,QT,ET,THT,EN,EDUM)
    IF(EN=ENTHG) 700,700,160
160 CALL DISTR(WT,THT,FT,NWT,10)
    DELTN=DELTA(0.0,0.0,0.0,DNO,0.0,0.0,0.0,0.0,X,Y,Z,RS,1)
    CALL INTRPL(MNT,ENT,SIGNT,EN,VSNT)
    ETAN=EXP(-VSNT*DELTN)
    FLUX=FT*ETAN*SIN(TH)*VOL1

    CALCULATE GAMMA PRODUCTION FROM POINT S(1)

    DG=SEPAR(X,Y,Z,0.0,YD,ZD)
    CALL INTRPL(MGP,EGP,SIGGP,EN,VSGP)
    IF(MWGP) 170,170,200
170 DSIGGP=VSGP/4.0/PI
    G0 T0 203
200 D0 202 I=1,MWGP
    M=NWGP(I)
    D0 201 J=1,M
    A(J)=EWGP(I,J)
201 B(J)=WGP(I,J)
202 CALL INTRPL(D,A,B,EN,WORK(I))
    CALL ANGLE(0,0,YD,ZD,X,Y,Z,X,Y,Z,0.0,0.0,0.0,0.0,THNG)
    CALL DISTR(WORK,THNG,SG,MWGP,10)
    DSIGGP=VSGP*SG/4.0/PI
203 DELTG=DELTA(0.0,0.0,0.0,DNO,0.0,YD,ZD,X,Y,Z,RS,1)

```

```
ETAG=EXP(-SIGG[*DELTS])
YLDG=FLUX*DSIGGP*ETAG/DG/DG
```

```
UPDATE YLDSUM(1)
```

```
YLDSUM(1)=YLDSUM(1)+YLDG
```

```
CHECK IF MULTIPLE SCATTERING CALCULATIONS ARE REQUESTED,
INITIALIZE PARAMETERS IF REQUIRED
```

```
IF(NSCAT-1) 240,700,240
```

```
240 ISCAT=2
```

```
XSAV1=0.0
```

```
YSAV1=0.0
```

```
ZSAV1=0.0
```

```
USAV=U
```

```
VSAV=V
```

```
WSAV=W
```

```
XSAV2=X
```

```
YSAV2=Y
```

```
ZSAV2=Z
```

```
DO 250 I=2,NSCAT
```

```
J=I-1
```

```
250 INDEX(J)=0
```

```
C
CXXX START OF MULTIPLE SCATTERING LOOP
```

```
SELECT SCATTERING POINT S(ISCAT)
```

```
300 R=RANF(-1)
```

```
RR=VALUE(R,0,0,RMAX)
```

```
R=RANF(-1)
```

```
TH=VALUE(R,0,0,PI)
```

```
R=RANF(-1)
```

```
PHI=VALUE(R,-PI,PI)
```

```
CALL TRANSF(USAV,VSAV,WSAV,TH,PHI,U,V,W)
```

```
X=XSAV2+RR*U
```

```
Y=YSAV2+RR*V
```

```
Z=ZSAV2+RR*W
```

```
IF(X+HD2) 700,700,350
```

```
350 IF(X-HD2) 351,700,700
```

```
351 ZMDNO=Z-DNO
```

```
TEST=Y*Y+ZMDNO*ZMDNO
```

```
IF(TEST-RSRS) 352,700,700
```

```
352 INDEX(ISCAT)=1
```

```
NHIT(ISCAT)=NHIT(ISCAT)+1
```

```
CALL ANGLE(X,Y,Z,XSAV2,YSAV2,ZSAV2,XSAV1,YSAV1,Z
1SAV1,THSCT)
```

```
SELECT NEUTRON SCATTERING PROCESS FOR POINT S(ISCAT-1)
```

```
DO 407 I=1,MNS
```

```
EB=-QNS(I)*(1.0+(1.0087/(A2NS(I)-1.0087))-(0.5*QNS(I)/(A2NS(I)-1.0
1087)/931.478))
```

```
IF(EN-EB) 400,400,401
```

```
400 DSIGNS(I)=0.0
```

```
GO TO 407
```

```
401 M=NNS(I)
```

```
DO 402 J=1,M
```

```
A(J)=ENS(I,J)
```

```

402 B(J)=SIGNS(I,J)
CALL INTRPL(M,A,B,EN,VSSCT)
IF(MWNS(I)) 403,403,404
403 DSIGNS(I)=VSSCT/4.0/PI
GO TO 407
404 M=MWNS(I)
DO 405 J=1,M
L=NWNS(I,J)
DO 405 K=1,L
A(K)=EWNS(I,J,K)
405 B(K)=WNS(I,J,K)
406 CALL INTRPL(L,A,B,EN,WORK(J))
CALL DISTR(WORK,THSCT,SSCT,M,10)
DSIGNS(I)=VSSCT*SSCT/4.0/PI
407 CONTINUE
SUMSCT=0.0
DO 408 I=1,MNS
408 SUMSCT=SUMSCT+DSIGNS(I)
IF(SUMSCT) 409,700,409
409 PSI(1)=0.0
K=MNS+1
PSI(K)=1.0
IF(MNS-1) 410,410,411
410 INDX=1
GO TO 414
411 SUMPSI=0.0
DO 413 I=2,MNS
J=I-1
SUMPSI=SUMPSI+DSIGNS(J)
PSI(I)=SUMPSI/SUMSCT
IF(PSI(I)-1.0) 412,412,412
412 PSI(I)=1.0
413 CONTINUE
R=RANF(-1)
CALL FINDI(PSI,K,6,R,INDX)
414 NLEV(INDX)=NLEV(INDX)+1

```

C  
C  
C

```

CALCULATE NEUTRON ENERGY AND FLUX AT POINT S(ISCAT)
200 ENSAV=EN
CALL KINAM(1.0087,A2NS(INDX),1.0087,QNS(INDX),ENSAV,THSCT,EN,EDUM)
IF(EN-ENTHG) 700,700,501
201 CALL INTRPL(MNT,ENT,SIGNT,EN,VSNT)
ETAN=EXF(-VSNT*RR)
FLUX=FLUX*SUMSCT*ETAN*SIN(TH)*V0LH

```

C  
C  
C

```

CALCULATE GAMMA PRODUCTION FROM POINT S(ISCAT)
DG=SEPAR(X,Y,Z,U,0,YD,ZD)
CALL INTRPL(MGP,EGP,SIGGP,EN,VSGP)
IF(MWGP) 502,502,500
202 DSIGGP=VSGP/4.0/PI
GO TO 503
300 DO 302 I=1,MWGP
M=NWGP(I)
DO 301 J=1,M
A(J)=EWGP(I,J)
301 B(J)=WGP(I,J)
302 CALL INTRPL(M,A,B,EN,WORK(I))
CALL ANGLE(0,0,YD,ZD,X,Y,Z,X,Y,Z,XSAV2,YS AV2,ZSAV2,THNG)

```



```

IF(NSCAT=1) 804,804.802
002 WRITE(5,803)
803 FORMAT(7HNLEV(I))
WRITE(5,703) (NLEV(I),I=1,MNS)
004 WRITE(5,805)
805 FORMAT(7HNHIT(I))
WRITE(5,703) (NHIT(I),I=1,NSCAT)
WRITE(5,806)
006 FORMAT(6HYLD(I))
WRITE(5,22) (YLD(I),I=1,NSCAT)
IF(NSCAT=1) 807,812,807
807 FYLD=YLD(1)
DO 808 I=1,NSCAT
008 YLD(I)=YLD(I)/FYLD
ALFA=0,0
DO 809 I=2,NSCAT
009 ALFA=ALFA+YLD(I)
WRITE(5,810)
010 FORMAT(17HNORMALIZED YLD(I))
WRITE(5,22) (YLD(I),I=1,NSCAT)
WRITE(5,811) ALFA
011 FORMAT(5HALFA=,E10,4)

```

```

C
012 CONTINUE
IF(K2=1) 1,813,1
813 PAUSE
GO TO 1
END
FUNCTION DELTA(X0,Y0,Z0,X1,Y1,Z1,X2,Y2,Z2,RS,INDEX)

```

```

C
C
C
C
C
C
FUNCTION TO DETERMINE PENETRATION DEPTH FOR R.C. CYLINDER.
INDEX=1,2 OR 3 IMPLIES CYLINDER AXIS PARALLEL TO X,Y-OR Z-AXIS
RESPECTIVELY. (X0,Y0,Z0) IS CYLINDER CENTER, (X1,Y1,Z1) IS
EXTERIOR POINT, (X2,Y2,Z2) IS INTERIOR POINT, RS=CYLINDER
RADIUS

```

```

R=SQRT((X2-X1)*(X2-X1)+(Y2-Y1)*(Y2-Y1)+(Z2-Z1)*(Z2-Z1))
A=(X2-X1)/R
B=(Y2-Y1)/R
C=(Z2-Z1)/R
GO TO(1,2,3),INDEX
1 Y0W=Y0
Z0W=Z0
Y1W=Y1
Z1W=Z1
BW=B
CW=C
GO TO 4
2 Y0W=Z0
Z0W=X0
Y1W=Z1
Z1W=X1
BW=C
CW=A
GO TO 4
3 Y0W=X0
Z0W=Y0
Y1W=X1
Z1W=Y1
BW=A

```

```

      CW=B
4  S=(BW*(Y0W-Y1W)+CW*(Z0W-Z1W)-SQRT(ABS((BW*BW+CW*CW)*RS*RS-(CW*(Y1W
1-Y0W)-BW*(Z1W-Z0W))*(CW*(Y1W-Y0W)-BW*(Z1W-Z0W)))))/(BW*BW+CW*CW)
      DELTA=R-S
      RETURN
      END
      SUBROUTINE KINAM(A1,A2,A3,Q,E1,TH3,E31,E32)

```

C

```

      W1=931,478*A1
      W2=931,478*A2
      W3=931,478*A3
      W4=W1+W2-W3-Q
      EF=-Q*(1.0+(W1/W2)-(0.5*Q/W2))
      EB=-Q*(1.0+(W1/(W2-W3))-(0.5*Q/(W2-W3)))
      IF(E1-EF) 1,1,2
1  E31=0,0
11 E32=0,0
      GO TO 6
2  C=COS(TH3)
      A=2.0*(W3+W4+E1+Q)
      B=2.0*E1*(W1-W4-Q)-(2.0*W4*Q+Q*Q)
      D=E1*(E1+2.0*W1)*C*C
      TERM=(B*B-2.0*W3*A*B+4.0*W3*W3*D)*E1*(E1+2.0*W1)
      IF(TERM) 1,1,3
3  DEN=A*A-4.0*D
      U=(4.0*W3*D-A*B)/DEN
      V=2.0*C*SQRT(ABS(TERM))/DEN
      E31=U+V
      IF(E1-EB) 4,4,5
4  IF(TH3-1.5707963) 41,11,11
41 E32=U-V
      GO TO 6
5  E32=E31
6  RETURN
      END

```

```

      SUBROUTINE ANGLE(X1H,Y1H,Z1H,X1T,Y1T,Z1T,X2H,Y2H,Z2H,X2T,Y2T,Z2T,T
1H)
      V1=SQRT(ABS((X1H-X1T)*(X1H-X1T)+(Y1H-Y1T)*(Y1H-Y1T)+(Z1H-Z1T)*(Z1H
1-Z1T)))
      V2=SQRT(ABS((X2H-X2T)*(X2H-X2T)+(Y2H-Y2T)*(Y2H-Y2T)+(Z2H-Z2T)*(Z2H
1-Z2T)))
      DOT=(X1H-X1T)*(X2H-X2T)+(Y1H-Y1T)*(Y2H-Y2T)+(Z1H-Z1T)*(Z2H-Z2T)
      CTH=DOT/V1/V2
      TH=ARCCOS(CTH,2)
      RETURN
      END

```

```

      SUBROUTINE DISTR(W,TH,V,NW,NMAX)
      DIMENSION W(NMAX)
      V=1,0
      IF(NW,EQ,0) GO TO 4
      DO 2 I=1,NW
      IF(W(I)) 21,20,21
20 VADD=0,0
      GO TO 22
21 VADD=W(I)*POLYL(2,I,TH)
22 V=V+VADD
2  CONTINUE
      IF(V) 3,4,4
3  V=0,0
4  RETURN

```

```

END
FUNCTION PØLYL(IØP,N,ANGLE)
X = ANGLE
GØ TØ (10,11,12),IØP
10 X = .017453293*X
11 X = CØS(X)
12 NØIG = N-1
IF(NØIG) 1,2,3
1 PØLYL = 1.0
GØ TØ 100
2 PØLYL = X
GØ TØ 100
3 PL = X
PLM1 = 1.0
DØ 4 L=1,NØIG
PØLYL = (FLØAT(2*L+1)*X*PL - FLØAT(L)*PLM1)/FLØAT(L+1)
PLM1 = PL
4 PL = PØLYL
100 RETURN
END

```

```

SUBROUTINE INTRPL(N,XT,YT,X,Y)
DIMENSION XT(N),YT(N)
IF(X=XT(1)) 1,3,4
1 WRITE(1,2)
2 FØRMAT(8HRANG ERR)
PAUSE
3 Y=YT(1)
GØ TØ 24
4 IF(X=XT(N)) 7,5,1
5 Y=YT(N)
GØ TØ 24
7 I=0
J=N
8 K=0,5*FLØAT(J-I)+0,1
K=K+I
IF(X=XT(K)) 9,10,11
9 J=K
GØ TØ 12
10 Y=YT(K)
GØ TØ 24
11 I=K
12 IF(J-I-1) 13,13,8
13 I=J
J=I-1
DEN=XT(J)-XT(I)
C1=(XT(J)*YT(I)-XT(I)*YT(J))/DEN
C2=(YT(J)-YT(I))/DEN
Y=C1+C2*X
24 RETURN
END

```

```

FUNCTION ARCCØS(X,K)
ARCCØS=1.5707963
IF(ABS(X),GT,.999999) X=.999999*X/ABS(X)
IF(X*X,GT,1,JE=70) ARCCØS=ATAN(SØRT(ABS(1,/(X/X-1,)))
IF(X,LT,0,) ARCCØS=3,1415926-ARCCØS
GØ TØ (100,200),K
100 ARCCØS=ARCCØS*57,2957795
200 RETURN
END
FUNCTION EXP(Z)

```

```

IF(Z) 1,1,3
1 IF(Z,LT,-70,0) Z=-70,0
  IF(Z,GT,-.1E-04) GO TO 2
  EXF=EXP(Z)
  GO TO 4
3 IF(Z,GT,70,0) Z=70,0
  IF(Z,LT,.1E-04) GO TO 2
  EXF=EXP(Z)
  GO TO 4
2 EXF=1,0+Z
4 CONTINUE
  RETURN
  END
SUBROUTINE FINDI(Y,N,NDIM,Z,IZ)
  DIMENSION Y(NDIM)
  NMIN=1
  NMAX=N
36 INTER=0,5*FLOAT(NMAX-NMIN)+0,1
  NTEST=NMIN+INTER
  IF(Z-Y(NTEST)) 1,2,3
  1 NMAX=NTEST
  GO TO 4
  2 IZ=NTEST
  GO TO 999
  3 NMIN=NTEST
  4 IF(NMAX-NMIN-1) 5,5,36
  5 IZ=NMAX-1
999 RETURN
  END
SUBROUTINE TRANSF(U,V,W,TH,PHI,UP,VP,WP)

```

C

```

A=COS(TH)
B=SIN(TH)
C=COS(PHI)
D=SIN(PHI)
TEST=1,0-ABS(W)
IF(TEST,GT,.1E-05) GO TO 1
UP=B*C
VP=B*D
WP=A*W
GO TO 2
1 CONTINUE
  FACT=SQRT(1,0-W*W)
  UP=((B*C*W*U-B*D*V)/FACT)+A*U
  VP=((B*C*W*V+B*D*U)/FACT)+A*V
  WP=-B*C*FACT+A*W
2 CONTINUE
  RETURN
  END

```

S

## REFERENCES

1. "Compilation of Requests for Nuclear Data," Report BNL-50444, compiled and edited by the National Neutron Cross Section Center for the U.S. Nuclear Data Committee, Brookhaven National Laboratory (1975).
2. CINDA - 75, Vol. 1, "An Index to the Literature on Microscopic Neutron Data," published by the International Atomic Energy Agency, Vienna (1975).
3. E. Barnard, J.A.M. deVilliers, C.A. Engelbrecht, D. Reitmann and A.B. Smith, Nucl. Phys. A118, 321 (1968).
4. J. K. Dickens, G. L. Morgan and F. G. Perey, "Neutron-Induced Gamma-Ray Production in Iron for the Energy Range  $0.8 \leq E_n \leq 20$  MeV," Report ORNL-TM-3850, Oak Ridge National Laboratory (1972).
5. V. J. Orphan, C. G. Hoot and Joseph John, Gulf Radiation Technology Report RT-A10743 (1971); and Proceedings of the Third Conference on Neutron Cross Sections and Technology, CONF-710301, Vol. 1, p. 227, U.S. Atomic Energy Commission, National Technical Information Service (1971).
6. E. Voss, S. Cierjacks and L. Kropp, Proceedings of the Third Conference on Neutron Cross Sections and Technology, CONF-710301, Vol. 1, p. 218, U.S. Atomic Energy Commission, National Technical Information Service (1971).
7. "Experimental Data File, CSISRS", National Neutron Cross Section Center, Brookhaven National Laboratory.
8. R. W. Benjamin, P.S. Buchanan and I. L. Morgan, Nucl. Phys. 79, 241 (1966).
9. Donald L. Smith, "A Spectrometer for the Investigation of Gamma Radiation Produced by Neutron-Induced Reactions," Report ANL/NDM-12, Argonne National Laboratory (1975).
10. Donald L. Smith, "Sample-Size Effects in Fast-Neutron Gamma-Ray Production Measurements: Solid Cylinder Samples," Report ANL/NDM-17, Argonne National Laboratory (1975).
11. J. W. Meadows and D. L. Smith, "Neutrons from Proton Bombardment of Natural Lithium," Report ANL-7938, Argonne National Laboratory (1972).
12. J. W. Meadows, Nucl. Sci. Eng. 49, 310 (1972).

13. Donald L. Smith and James W. Meadows, "Response of Several Threshold Reactions in Reference Fission Neutron Fields," Report ANL/NDM-13, Argonne National Laboratory (1975).
14. W. P. Poenitz and J. F. Whalen, "On-Line Computer Facility and Operating System COSACS at the ANL Fast Neutron Generator", Report ANL-8026, Argonne National Laboratory (1973).
15. "Evaluated Neutron Data File, ENDF/B-IV", National Neutron Cross Section Center, Brookhaven National Laboratory (1975).
16. E. Storm and H. I. Israel, Nuclear Data Tables A7, 565 (1970).
17. A. B. Smith, Argonne National Laboratory (Private Communication, 1976).
18. E. D. Cashwell, C. J. Everett and O. W. Rechard, "A Practical Manual on the Monte Carlo Method for Random Walk Problems", Report No. LA-2120, Los Alamos Scientific Laboratory (1957).

Table I

Major Sources of Uncertainty in the  
Measured Cross Section Ratios

<u>Source of Uncertainty</u>	<u>Magnitude (%)</u>
1. Determination of detector counts	
i) 0.847-MeV gamma ray	5
ii) 1.408-MeV gamma ray	10
2. Geometric effects	3
3. Neutron source characteristics	2
4. Gamma-ray detector efficiency	4
5. Mass of uranium deposit	1
6. Gamma-ray absorption in iron sample	5
7. Neutron absorption in iron sample	5
8. Neutron multiple scattering in iron sample	5
Total uncertainty <sup>a</sup>	
i) 0.847-MeV gamma ray	11
ii) 1.408-MeV gamma ray	14

<sup>a</sup> Total uncertainty is the root-mean-square composite of the listed partial uncertainties.

Table II

Measured Cross Section Ratios and Resultant  
Elemental Differential Cross Sections for Production  
of the 0.847-MeV Gamma Ray by Neutron Inelastic  
Scattering from Iron

$\langle\theta\rangle = 87.9$  Degrees

$E_n$ (MeV)	Resolution (MeV)	$[(d\sigma/d\Omega)/\sigma_{F,235}]^a$ (sr <sup>-1</sup> )	$(\frac{d\sigma}{d\Omega})^b$ (b/sr)
0.887	0.047	(5.66 ± 0.62)x 10 <sup>-3</sup>	(6.61 ± 0.79)x 10 <sup>-3</sup>
0.937	0.047	(7.25 ± 0.80)x 10 <sup>-3</sup>	(8.61 ± 1.03)x 10 <sup>-3</sup>
0.990	0.046	(1.36 ± 0.15)x 10 <sup>-2</sup>	(1.64 ± 0.20)x 10 <sup>-2</sup>
1.041	0.046	(1.38 ± 0.15)x 10 <sup>-2</sup>	(1.70 ± 0.20)x 10 <sup>-2</sup>
1.041	0.046	(1.57 ± 0.17)x 10 <sup>-2</sup>	(1.93 ± 0.23)x 10 <sup>-2</sup>
1.093	0.045	(2.28 ± 0.25)x 10 <sup>-2</sup>	(2.85 ± 0.34)x 10 <sup>-2</sup>
1.145	0.045	(2.26 ± 0.25)x 10 <sup>-2</sup>	(2.83 ± 0.34)x 10 <sup>-2</sup>
1.196	0.045	(1.94 ± 0.21)x 10 <sup>-2</sup>	(2.43 ± 0.29)x 10 <sup>-2</sup>
1.248	0.044	(2.30 ± 0.25)x 10 <sup>-2</sup>	(2.88 ± 0.35)x 10 <sup>-2</sup>
1.300	0.044	(1.96 ± 0.22)x 10 <sup>-2</sup>	(2.46 ± 0.30)x 10 <sup>-2</sup>

$\langle\theta\rangle = 52.9$  Degrees

$E_n$ (MeV)	Resolution (MeV)	$[(d\sigma/d\Omega)/\sigma_{F,235}]^a$ (sr <sup>-1</sup> )	$(\frac{d\sigma}{d\Omega})^b$ (b/sr)
0.879	0.073	(1.31 ± 0.14)x 10 <sup>-2</sup>	(1.52 ± 0.18)x 10 <sup>-2</sup>
0.902	0.072	(9.89 ± 1.09)x 10 <sup>-3</sup>	(1.16 ± 0.14)x 10 <sup>-2</sup>
0.919	0.072	(1.50 ± 0.17)x 10 <sup>-2</sup>	(1.77 ± 0.21)x 10 <sup>-2</sup>
0.969	0.071	(2.07 ± 0.23)x 10 <sup>-2</sup>	(2.49 ± 0.30)x 10 <sup>-2</sup>
1.014	0.070	(2.78 ± 0.31)x 10 <sup>-2</sup>	(3.39 ± 0.41)x 10 <sup>-2</sup>
1.014	0.070	(2.58 ± 0.28)x 10 <sup>-2</sup>	(3.14 ± 0.38)x 10 <sup>-2</sup>
1.066	0.070	(2.77 ± 0.30)x 10 <sup>-2</sup>	(3.44 ± 0.41)x 10 <sup>-2</sup>
1.102	0.069	(2.94 ± 0.32)x 10 <sup>-2</sup>	(3.68 ± 0.44)x 10 <sup>-2</sup>
1.116	0.069	(3.24 ± 0.36)x 10 <sup>-2</sup>	(4.05 ± 0.49)x 10 <sup>-2</sup>
1.167	0.068	(3.43 ± 0.38)x 10 <sup>-2</sup>	(4.30 ± 0.52)x 10 <sup>-2</sup>
1.218	0.068	(2.81 ± 0.31)x 10 <sup>-2</sup>	(3.52 ± 0.42)x 10 <sup>-2</sup>
1.260	0.067	(2.34 ± 0.26)x 10 <sup>-2</sup>	(2.93 ± 0.35)x 10 <sup>-2</sup>
1.303	0.066	(2.57 ± 0.28)x 10 <sup>-2</sup>	(3.22 ± 0.39)x 10 <sup>-2</sup>
1.312	0.067	(2.40 ± 0.26)x 10 <sup>-2</sup>	(3.01 ± 0.36)x 10 <sup>-2</sup>
1.364	0.066	(3.61 ± 0.40)x 10 <sup>-2</sup>	(4.53 ± 0.54)x 10 <sup>-2</sup>
1.416	0.066	(3.90 ± 0.43)x 10 <sup>-2</sup>	(4.90 ± 0.59)x 10 <sup>-2</sup>
1.467	0.065	(4.11 ± 0.45)x 10 <sup>-2</sup>	(5.18 ± 0.62)x 10 <sup>-2</sup>
1.502	0.064	(4.43 ± 0.49)x 10 <sup>-2</sup>	(5.58 ± 0.67)x 10 <sup>-2</sup>
1.519	0.065	(4.83 ± 0.53)x 10 <sup>-2</sup>	(6.08 ± 0.73)x 10 <sup>-2</sup>
1.519	0.064	(4.80 ± 0.53)x 10 <sup>-2</sup>	(6.05 ± 0.73)x 10 <sup>-2</sup>
1.569	0.065	(4.58 ± 0.50)x 10 <sup>-2</sup>	(5.77 ± 0.69)x 10 <sup>-2</sup>
1.621	0.064	(4.84 ± 0.53)x 10 <sup>-2</sup>	(6.11 ± 0.73)x 10 <sup>-2</sup>
1.663	0.064	(4.89 ± 0.54)x 10 <sup>-2</sup>	(6.18 ± 0.74)x 10 <sup>-2</sup>
1.714	0.064	(3.79 ± 0.42)x 10 <sup>-2</sup>	(4.79 ± 0.57)x 10 <sup>-2</sup>

Table II (Cont'd)

<θ> = 52.9 Degrees (Cont'd)

$E_n$ (MeV)	Resolution (MeV)	$[(d\sigma/d\Omega)/\sigma_{F,235}]^a$ (sr <sup>-1</sup> )	$(\frac{d\sigma}{d\Omega})^b$ (b/sr)
1.766	0.063	$(3.93 \pm 0.43) \times 10^{-2}$	$(4.97 \pm 0.60) \times 10^{-2}$
1.803	0.062	$(3.48 \pm 0.38) \times 10^{-2}$	$(4.41 \pm 0.53) \times 10^{-2}$
1.817	0.063	$(3.16 \pm 0.35) \times 10^{-2}$	$(4.01 \pm 0.48) \times 10^{-2}$
1.870	0.063	$(5.29 \pm 0.58) \times 10^{-2}$	$(6.71 \pm 0.81) \times 10^{-2}$
1.920	0.062	$(3.96 \pm 0.44) \times 10^{-2}$	$(5.03 \pm 0.60) \times 10^{-2}$
1.971	0.062	$(5.15 \pm 0.57) \times 10^{-2}$	$(6.54 \pm 0.78) \times 10^{-2}$
2.001	0.061	$(5.19 \pm 0.57) \times 10^{-2}$	$(6.60 \pm 0.79) \times 10^{-2}$
2.022	0.061	$(5.33 \pm 0.59) \times 10^{-2}$	$(6.78 \pm 0.81) \times 10^{-2}$
2.022	0.062	$(5.45 \pm 0.60) \times 10^{-2}$	$(6.93 \pm 0.83) \times 10^{-2}$

<sup>a</sup> Errors correspond to ± 11%.

<sup>b</sup> Differential cross sections are computed using ENDF/B-IV [15] values for the <sup>235</sup>U fission cross section. Errors correspond to ± 12%.

Table III

Measured Angular Distributions for the 0.847-  
MeV Gamma Ray from the  $^{56}\text{Fe}(n,n'\gamma)^{56}\text{Fe}$  Reaction

$E_n = 0.93 \text{ MeV}$

$\theta$ (deg)	$\cos \theta$ (no dim)	$[W(\theta)/W(90^\circ)]$ (no dim) <sup>a</sup>
28.9	0.8755	
38.3	0.7848	$2.37 \pm 0.12$
47.9	0.6704	$2.47 \pm 0.12$
57.7	0.5344	$2.30 \pm 0.12$
67.6	0.3811	$2.04 \pm 0.10$
77.6	0.2147	$1.60 \pm 0.08$
87.8	0.0384	$1.22 \pm 0.06$
98.1	-0.1409	$1.03 \pm 0.05$
108.3	-0.3140	$1.08 \pm 0.05$
118.5	-0.4772	$1.44 \pm 0.07$
128.7	-0.6252	$1.95 \pm 0.10$
133.8	-0.6921	$2.36 \pm 0.12$
		$2.53 \pm 0.13$

$E_n = 0.98 \text{ MeV}$

$\theta$ (deg)	$\cos \theta$ (no dim)	$[W(\theta)/W(90^\circ)]$ (no dim) <sup>a</sup>
28.9	0.8755	
38.4	0.7837	$2.15 \pm 0.11$
48.0	0.6691	$2.13 \pm 0.11$
57.7	0.5344	$1.99 \pm 0.10$
67.6	0.3811	$1.69 \pm 0.08$
77.7	0.2130	$1.41 \pm 0.07$
87.8	0.0384	$1.15 \pm 0.06$
98.0	-0.1392	$1.01 \pm 0.05$
108.2	-0.3123	$1.06 \pm 0.05$
118.5	-0.4772	$1.27 \pm 0.06$
128.6	-0.6239	$1.63 \pm 0.08$
133.7	-0.6909	$1.92 \pm 0.10$
		$2.01 \pm 0.10$

$E_n = 1.08 \text{ MeV}$

$\theta$ (deg)	$\cos \theta$ (no dim)	$[W(\theta)/W(90^\circ)]$ (no dim) <sup>a</sup>
28.9	0.8755	
38.4	0.7837	$1.74 \pm 0.09$
48.0	0.6691	$1.70 \pm 0.08$
		$1.52 \pm 0.08$

Table III (Cont'd)

 $E_n = 1.08 \text{ MeV (Cont'd)}$ 

$\theta$ (deg)	$\cos \theta$ (no dim)	$[W(\theta)/W(90^\circ)]$ (no dim) <sup>a</sup>
57.8	0.5329	1.38 ± 0.07
67.7	0.3795	1.22 ± 0.06
77.7	0.2130	1.07 ± 0.05
87.8	0.0384	1.00 ± 0.05
98.0	-0.1392	1.05 ± 0.05
108.2	-0.3123	1.13 ± 0.06
118.4	-0.4756	1.35 ± 0.07
128.6	-0.6239	1.52 ± 0.08
133.7	-0.6909	1.60 ± 0.08

 $E_n = 1.18 \text{ MeV}$ 

$\theta$ (deg)	$\cos \theta$ (no dim)	$[W(\theta)/W(90^\circ)]$ (no dim) <sup>a</sup>
29.0	0.8746	1.84 ± 0.09
38.4	0.7837	1.83 ± 0.09
48.0	0.6691	1.69 ± 0.08
57.8	0.5329	1.56 ± 0.08
67.7	0.3795	1.32 ± 0.07
77.7	0.2130	1.13 ± 0.06
87.8	0.0384	1.00 ± 0.05
98.0	-0.1392	1.05 ± 0.05
108.2	-0.3123	1.27 ± 0.06
118.4	-0.4756	1.51 ± 0.08
128.6	-0.6239	1.82 ± 0.09
133.6	-0.6896	1.90 ± 0.10

 $E_n = 1.28 \text{ MeV}$ 

$\theta$ (deg)	$\cos \theta$ (no dim)	$[W(\theta)/W(90^\circ)]$ (no dim) <sup>a</sup>
29.0	0.8746	1.43 ± 0.07
38.4	0.7837	1.29 ± 0.06
48.0	0.6691	1.19 ± 0.06
57.8	0.5329	1.14 ± 0.06
67.7	0.3795	1.06 ± 0.05
87.8	0.0384	1.01 ± 0.05
97.9	-0.1374	1.00 ± 0.05
118.3	-0.4741	1.13 ± 0.06
128.5	-0.6225	1.19 ± 0.06
133.6	-0.6896	1.30 ± 0.07

Table III (Cont'd)

 $E_n = 1.38 \text{ MeV}$ 

$\theta$ (deg)	$\cos \theta$ (no dim)	$[W(\theta)/W(90^\circ)]$ (no dim) <sup>a</sup>
29.0	0.8746	1.56 ± 0.08
38.4	0.7837	1.42 ± 0.07
48.1	0.6678	1.28 ± 0.06
57.8	0.5329	1.18 ± 0.06
67.7	0.3795	1.10 ± 0.05
77.7	0.2130	1.04 ± 0.05
87.8	0.0384	0.97 ± 0.05
97.9	-0.1374	1.02 ± 0.05
108.1	-0.3107	1.07 ± 0.05
118.3	-0.4741	1.14 ± 0.06
128.5	-0.6225	1.24 ± 0.06
133.6	-0.6896	1.28 ± 0.06

 $E_n = 1.59 \text{ MeV}$ 

$\theta$ (deg)	$\cos \theta$ (no dim)	$[W(\theta)/W(90^\circ)]$ (no dim) <sup>a</sup>
29.0	0.8746	1.57 ± 0.08
38.5	0.7826	1.48 ± 0.07
48.1	0.6678	1.42 ± 0.07
57.8	0.5329	1.32 ± 0.07
67.7	0.3795	1.22 ± 0.06
77.7	0.2130	1.06 ± 0.05
87.8	0.0384	1.00 ± 0.05
97.9	-0.1374	1.00 ± 0.05
108.1	-0.3107	1.15 ± 0.06
118.3	-0.4741	1.29 ± 0.06
128.5	-0.6225	1.40 ± 0.07
133.6	-0.6896	1.47 ± 0.07

 $E_n = 1.68 \text{ MeV}$ 

$\theta$ (deg)	$\cos \theta$ (no dim)	$[W(\theta)/W(90^\circ)]$ (no dim) <sup>a</sup>
29.0	0.8746	1.38 ± 0.07
38.5	0.7826	1.34 ± 0.07
48.1	0.6678	1.32 ± 0.07
57.9	0.5314	1.24 ± 0.06
67.7	0.3795	1.15 ± 0.06
77.7	0.2130	1.05 ± 0.05
87.8	0.0384	1.00 ± 0.05
97.9	-0.1374	1.02 ± 0.05
108.1	-0.3107	1.10 ± 0.05
118.3	-0.4741	1.21 ± 0.06
128.5	-0.6225	1.32 ± 0.07
133.6	-0.6896	1.36 ± 0.07

Table III (Cont'd)

 $E_n = 1.79 \text{ MeV}$ 

$\theta$ (deg)	$\cos \theta$ (no dim)	$[W(\theta)/W(90^\circ)]$ (no dim) <sup>a</sup>
29.0	0.8746	$1.32 \pm 0.07$
38.5	0.7826	$1.29 \pm 0.06$
57.9	0.5314	$1.17 \pm 0.06$
67.8	0.3778	$1.09 \pm 0.05$
77.8	0.2113	$1.05 \pm 0.05$
87.8	0.0384	$0.99 \pm 0.05$
97.9	-0.1374	$1.01 \pm 0.05$
118.3	-0.4741	$1.15 \pm 0.06$
133.6	-0.6896	$1.26 \pm 0.06$

 $E_n = 1.85 \text{ MeV}$ 

$\theta$ (deg)	$\cos \theta$ (no dim)	$[W(\theta)/W(90^\circ)]$ (no dim) <sup>a</sup>
29.0	0.8746	$1.34 \pm 0.07$
38.5	0.7826	$1.39 \pm 0.07$
48.1	0.6678	$1.32 \pm 0.07$
53.4	0.5962	$1.24 \pm 0.06$
67.8	0.3778	$1.15 \pm 0.06$
77.7	0.2130	$1.04 \pm 0.05$
87.8	0.0384	$1.01 \pm 0.05$
97.9	-0.1374	$1.02 \pm 0.05$
108.1	-0.3107	$1.04 \pm 0.05$
118.3	-0.4741	$1.15 \pm 0.06$
128.5	-0.6225	$1.24 \pm 0.06$
133.6	-0.6896	$1.25 \pm 0.06$

 $E_n = 2.03 \text{ MeV}$ 

$\theta$ (deg)	$\cos \theta$ (no dim)	$[W(\theta)/W(90^\circ)]$ (no dim) <sup>a</sup>
29.0	0.8746	$1.26 \pm 0.06$
38.5	0.7826	$1.18 \pm 0.06$
48.1	0.6678	$1.14 \pm 0.06$
57.9	0.5314	$1.12 \pm 0.06$
67.7	0.3795	$1.05 \pm 0.05$
77.7	0.2130	$1.00 \pm 0.05$
87.7	0.0401	$1.01 \pm 0.05$
97.9	-0.1374	$1.02 \pm 0.05$
108.1	-0.3107	$1.04 \pm 0.05$
118.3	-0.4741	$1.09 \pm 0.05$
128.5	-0.6225	$1.17 \pm 0.06$
133.6	-0.6896	$1.18 \pm 0.06$

<sup>a</sup> Errors correspond to  $\pm 5\%$ .

Table IV

$\omega$  Coefficients Derived from Least-Squares Fits of a Legendre Polynomial Expansion to Measured Angular Distributions for the 0.847-MeV Gamma Ray from the  $^{56}\text{Fe}(n,n'\gamma)^{56}\text{Fe}$  Reaction <sup>a</sup>

$E_n$ (MeV)	$\omega_2^b$ (no dim)	$\omega_4^b$ (no dim)
0.93	0.521 ± 0.030	-(0.511 ± 0.033)
0.98	0.539 ± 0.013	-(0.302 ± 0.014)
1.08	0.435 ± 0.017	-(0.144 ± 0.019)
1.18	0.398 ± 0.039	-(0.331 ± 0.044)
1.28	0.312 ± 0.031	0.020 ± 0.004
1.38	0.396 ± 0.018	0.039 ± 0.020
1.59	0.319 ± 0.022	-(0.167 ± 0.025)
1.68	0.226 ± 0.012	-(0.155 ± 0.015)
1.79	0.216 ± 0.010	-(0.082 ± 0.013)
1.85	0.245 ± 0.031	-(0.089 ± 0.036)
2.03	0.190 ± 0.018	-(0.023 ± 0.021)

<sup>a</sup> Eq. (12) is used to fit angular distribution data.

<sup>b</sup> Errors are computed standard deviations.

Table V

Integrated Cross Sections for Production  
of the 0.847-MeV Gamma Ray by Neutron  
Inelastic Scattering from Iron

Values derived from 87.9-degree  
differential cross section data:

$E_n^a$ (MeV)	Resolution <sup>a</sup> (MeV)	$\omega_2^b$ (no dim)	$\omega_4^b$ (no dim)	$(\frac{d\sigma}{d\Omega})^a$ (barn/sr)	$\sigma^c$ (barn)	$\sigma/4\pi(d\sigma/d\Omega)_{55^\circ}^d$ (no dim)
0.887	0.047	0.506	-0.543	0.00661	0.151 ± 0.018	0.829
0.937	0.047	0.528	-0.432	0.00861	0.185 ± 0.022	0.860
0.990	0.046	0.515	-0.266	0.0164	0.317 ± 0.039	0.910
1.041	0.046	0.462	-0.185	0.017	0.301 ± 0.036	0.936
1.041	0.046	0.462	-0.185	0.0193	0.344 ± 0.041	0.936
1.093	0.045	0.425	-0.195	0.0285	0.495 ± 0.060	0.933
1.145	0.045	0.405	-0.294	0.0283	0.512 ± 0.061	0.901
1.196	0.045	0.371	-0.222	0.0243	0.413 ± 0.049	0.923
1.248	0.044	0.326	-0.036	0.0288	0.436 ± 0.052	0.988
1.300	0.044	0.342	0.027	0.0246	0.365 ± 0.044	1.013

Values derived from 52.9-degree  
differential cross section data:

$E_n^a$ (MeV)	Resolution <sup>a</sup> (MeV)	$\omega_2^b$ (no dim)	$\omega_4^b$ (no dim)	$(\frac{d\sigma}{d\Omega})^a$ (barn/sr)	$\sigma^c$ (barn)	$\sigma/4\pi(d\sigma/d\Omega)_{55^\circ}^d$ (no dim)
0.879	0.073	0.503	-0.551	0.0152	0.153 ± 0.018	0.827
0.902	0.072	0.513	-0.528	0.0116	0.117 ± 0.014	0.833
0.919	0.072	0.521	-0.507	0.0177	0.180 ± 0.021	0.839
0.969	0.071	0.537	-0.299	0.0249	0.273 ± 0.031	0.900
1.014	0.070	0.490	-0.228	0.0339	0.383 ± 0.045	0.922
1.014	0.070	0.490	-0.228	0.0314	0.355 ± 0.042	0.922
1.066	0.070	0.435	-0.144	0.0344	0.399 ± 0.047	0.950
1.102	0.069	0.422	-0.211	0.0368	0.418 ± 0.050	0.927
1.116	0.069	0.416	-0.239	0.0405	0.456 ± 0.055	0.918
1.167	0.068	0.396	-0.324	0.043	0.470 ± 0.056	0.891
1.218	0.068	0.352	-0.142	0.0352	0.411 ± 0.049	0.950
1.260	0.067	0.315	0.006	0.0293	0.364 ± 0.044	1.004
1.303	0.066	0.345	0.027	0.0322	0.402 ± 0.049	1.013
1.312	0.067	0.353	0.029	0.0301	0.377 ± 0.046	1.014
1.364	0.066	0.396	0.038	0.0453	0.568 ± 0.068	1.018
1.416	0.066	0.377	-0.013	0.049	0.603 ± 0.073	0.998
1.467	0.065	0.358	-0.064	0.0518	0.624 ± 0.074	0.978
1.502	0.064	0.345	-0.098	0.0558	0.663 ± 0.080	0.966
1.519	0.065	0.338	-0.115	0.0608	0.719 ± 0.087	0.960
1.519	0.064	0.338	-0.115	0.0605	0.715 ± 0.086	0.960
1.569	0.065	0.320	-0.164	0.0577	0.670 ± 0.080	0.942
1.621	0.064	0.267	-0.160	0.0611	0.713 ± 0.085	0.943
1.663	0.064	0.226	-0.154	0.0618	0.724 ± 0.086	0.945
1.714	0.064	0.221	-0.120	0.0479	0.567 ± 0.068	0.957
1.766	0.063	0.217	-0.085	0.0497	0.598 ± 0.072	0.970

Table V (Cont'd)

Values derived from 52.9-degree differential cross section data (Cont'd):

$E_n^a$ (MeV)	Resolution <sup>a</sup> (MeV)	$\omega_2^b$ (no dim)	$\omega_4^b$ (no dim)	$(\frac{d\sigma}{d\Omega})^a$ (barn/sr)	$\sigma^c$ (barn)	$\sigma/4\pi(d\sigma/d\Omega)_{55^\circ}^d$ (no dim)
1.803	0.062	0.232	-0.086	0.0441	$0.529 \pm 0.063$	0.969
1.817	0.063	0.238	-0.087	0.0401	$0.481 \pm 0.057$	0.969
1.870	0.063	0.233	-0.075	0.0671	$0.810 \pm 0.097$	0.974
1.920	0.062	0.218	-0.056	0.0503	$0.612 \pm 0.073$	0.980
1.971	0.062	0.202	-0.038	0.0654	$0.801 \pm 0.097$	0.987
2.001	0.061	0.193	-0.027	0.066	$0.813 \pm 0.097$	0.991
2.022	0.061	0.185	-0.019	0.0678	$0.840 \pm 0.101$	0.994
2.022	0.062	0.185	-0.019	0.0693	$0.857 \pm 0.103$	0.994

<sup>a</sup> Values reproduced from Table II.

<sup>b</sup> Obtained from linear interpolation of Table IV.

<sup>c</sup> Computed from Eq. (12). Errors correspond to  $\pm 12\%$ .

<sup>d</sup> This ratio indicates the importance of the  $P_4$  term. The ratio is unity if  $\omega_4 = 0$ .

Table VI

Measured Cross Section Ratios and Resultant  
Elemental Cross Sections for Production of the  
1.408-MeV Gamma Ray by Neutron Inelastic  
Scattering from Iron

$E_n$ (MeV)	Resolution (MeV)	$[(d\sigma/d\Omega)/\sigma_{F,235}]^a$ (sr <sup>-1</sup> )	$(\frac{d\sigma}{d\Omega})^b$ (barn/sr)	$\sigma = 4\pi (\frac{d\sigma}{d\Omega})^c$ (barn)
1.470	0.055	$(1.68 \pm 0.24) \times 10^{-3}$	$(2.12 \pm 0.31) \times 10^{-3}$	$(2.66 \pm 0.40) \times 10^{-2}$
1.522	0.055	$(1.75 \pm 0.24) \times 10^{-3}$	$(2.20 \pm 0.33) \times 10^{-3}$	$(2.76 \pm 0.41) \times 10^{-2}$
1.522	0.055	$(1.44 \pm 0.20) \times 10^{-3}$	$(1.81 \pm 0.27) \times 10^{-3}$	$(2.28 \pm 0.35) \times 10^{-2}$
1.571	0.055	$(1.78 \pm 0.25) \times 10^{-3}$	$(2.24 \pm 0.34) \times 10^{-3}$	$(2.81 \pm 0.42) \times 10^{-2}$
1.622	0.055	$(1.81 \pm 0.25) \times 10^{-3}$	$(2.29 \pm 0.34) \times 10^{-3}$	$(2.88 \pm 0.43) \times 10^{-2}$
1.664	0.055	$(2.11 \pm 0.30) \times 10^{-3}$	$(2.65 \pm 0.40) \times 10^{-3}$	$(3.34 \pm 0.50) \times 10^{-2}$
1.715	0.054	$(1.53 \pm 0.21) \times 10^{-3}$	$(1.94 \pm 0.29) \times 10^{-3}$	$(2.44 \pm 0.36) \times 10^{-2}$
1.767	0.054	$(1.59 \pm 0.22) \times 10^{-3}$	$(2.00 \pm 0.30) \times 10^{-3}$	$(2.52 \pm 0.38) \times 10^{-2}$
1.816	0.054	$(2.47 \pm 0.35) \times 10^{-3}$	$(3.13 \pm 0.47) \times 10^{-3}$	$(3.94 \pm 0.59) \times 10^{-2}$
1.869	0.054	$(1.95 \pm 0.27) \times 10^{-3}$	$(2.47 \pm 0.37) \times 10^{-3}$	$(3.11 \pm 0.47) \times 10^{-2}$
1.920	0.054	$(2.86 \pm 0.40) \times 10^{-3}$	$(3.64 \pm 0.55) \times 10^{-3}$	$(4.57 \pm 0.68) \times 10^{-2}$
1.971	0.053	$(2.62 \pm 0.37) \times 10^{-3}$	$(3.33 \pm 0.50) \times 10^{-3}$	$(4.18 \pm 0.63) \times 10^{-2}$
2.022	0.053	$(2.67 \pm 0.37) \times 10^{-3}$	$(3.38 \pm 0.51) \times 10^{-3}$	$(4.25 \pm 0.64) \times 10^{-2}$
2.022	0.053	$(2.97 \pm 0.42) \times 10^{-3}$	$(3.78 \pm 0.57) \times 10^{-3}$	$(4.75 \pm 0.72) \times 10^{-2}$

17.24

<sup>a</sup> Errors correspond to  $\pm 14\%$ .

<sup>b</sup> Differential cross section at 54.0 degrees is computed using ENDF/B-IV [15] values for the <sup>235</sup>U fission cross section. Errors correspond to  $\pm 15\%$ .

<sup>c</sup> Since no angular distribution data is available, the integrated cross section is approximated by  $4\pi$  times the measured differential cross section at 54.0 degrees. Errors correspond to  $\pm 15\%$ .

## FIGURE CAPTIONS

- Fig. 1. Plot of  $4\pi$  times the measured differential cross sections for production of 0.847-MeV gamma rays near 55 degrees via the  $^{56}\text{Fe}(n,n'\gamma)^{56}\text{Fe}$  reaction. The smoothed ENDF/B-IV [15] evaluation for the corresponding inelastic scattering cross section (Fig. 2) is superimposed for comparison. (ANL Neg. No. 116-76-63)
- Fig. 2. Plot of ENDF/B-IV [15] evaluated cross sections for excitation of the 0.847-MeV level in  $^{56}\text{Fe}$  via neutron inelastic scattering. The solid curve is plotted directly from the evaluation. The dotted curve corresponds to a smoothed version of the evaluation with 50-keV resolution. (ANL Neg. No. 116-76-32)
- Fig. 3. Angular distributions for the 0.847-MeV gamma ray. Data points are from the present experiment. Solid curves are best fits of Eq. (12) to the data. (ANL Neg. No. 116-76-7. Rev.1)
- Fig. 4. Plot of integrated cross section values for production of the 0.847-MeV gamma ray derived from differential cross section and angular distribution data acquired in the present experiment. Neutron energies at which angular distribution measurements were made are indicated by arrows. The smoothed ENDF/B-IV [15] evaluation (Fig. 2) is plotted for comparison. (ANL Neg. No. 116-76-37. Rev 1)
- Fig. 5. Plot of experimental data from the literature for neutron inelastic scattering from iron ( $Q = -0.847$  MeV) and production of the 0.847-MeV gamma ray. Data obtained from the CSISRS File at the National Neutron Cross Section Center [7]. The smoothed ENDF/B-IV [15] evaluation (Fig. 2) is superimposed for comparison. (ANL Neg. No. 116-76-33)

Fig. 6. Plot of  $4\pi$  times the measured differential cross sections for production of 1.408-MeV gamma rays near 55 degrees via the  $^{54}\text{Fe}(n,n'\gamma)^{54}\text{Fe}$  reaction. The ENDF/B-IV [15] evaluation for the corresponding inelastic scattering cross section is superimposed for comparison.

(ANL Neg. No. 116-76-38 Rev 1)

Fig. 7. Plot of experimental data from the literature for neutron inelastic scattering from iron ( $Q = -1.408$  MeV) and production of the 1.408-MeV gamma ray. Data obtained from the CSISRS File at the National Neutron Cross Section Center [7]. The ENDF/B-IV [15] evaluation is superimposed for comparison.

(ANL Neg. No. 116-76-45)

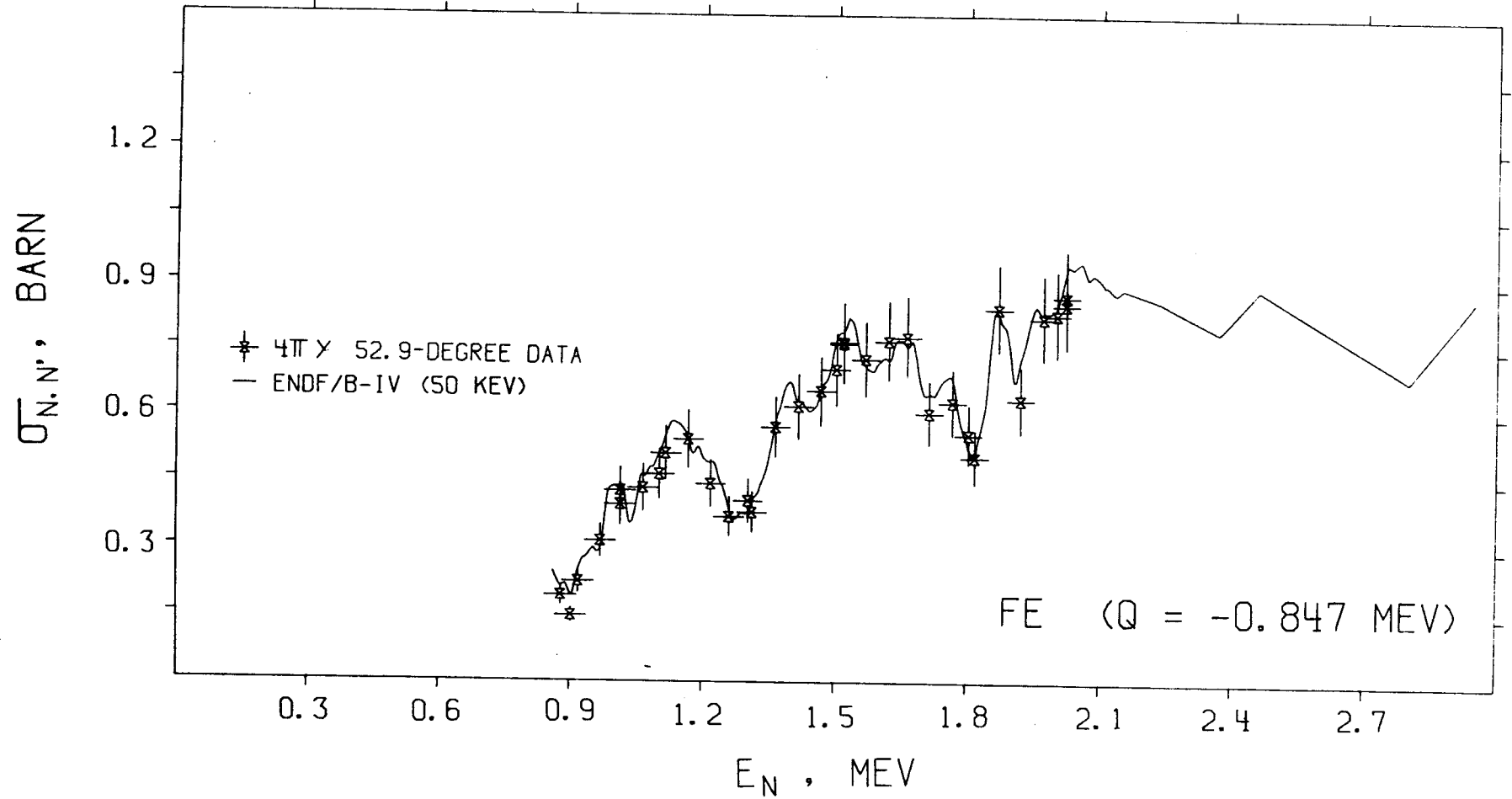


Figure 1

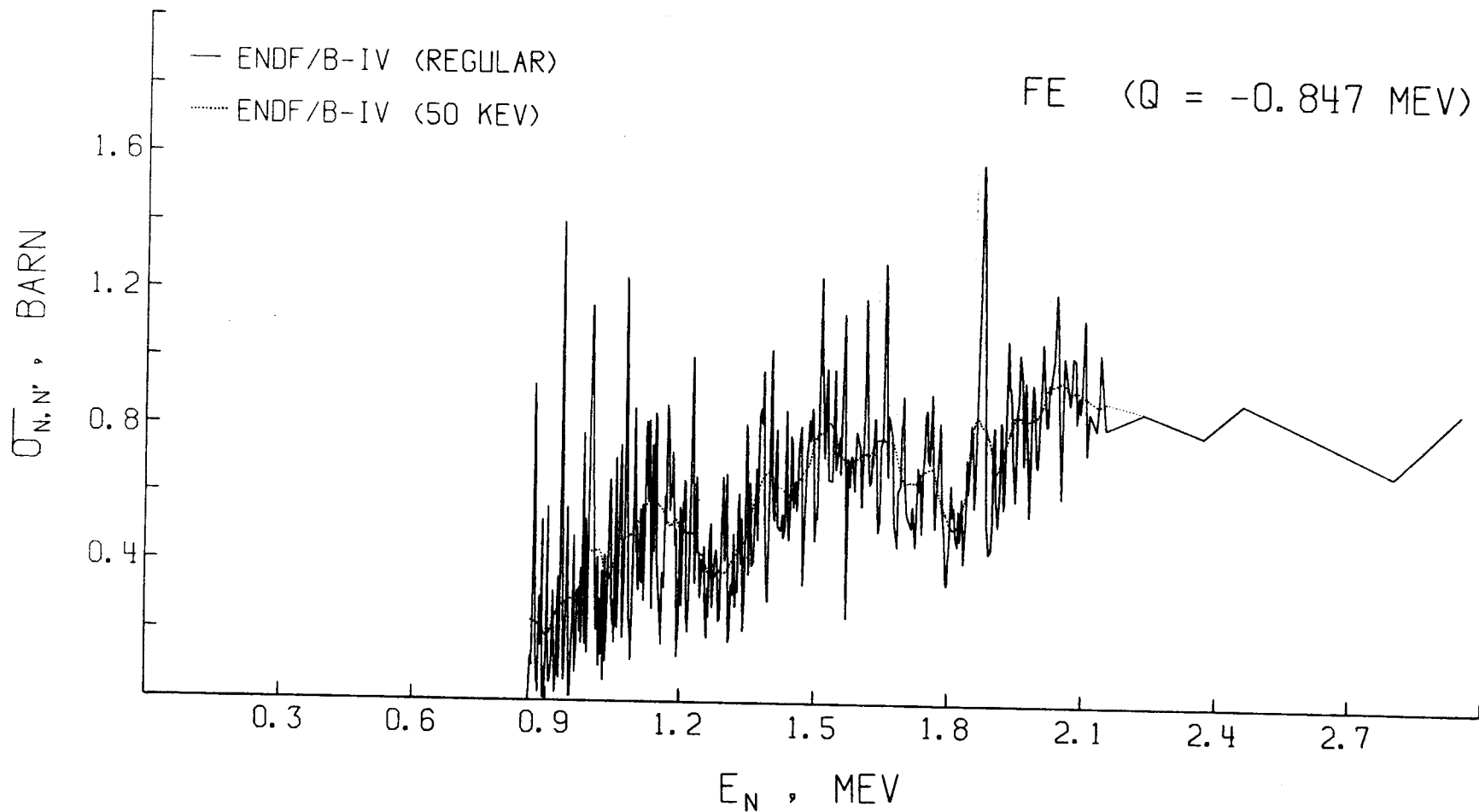
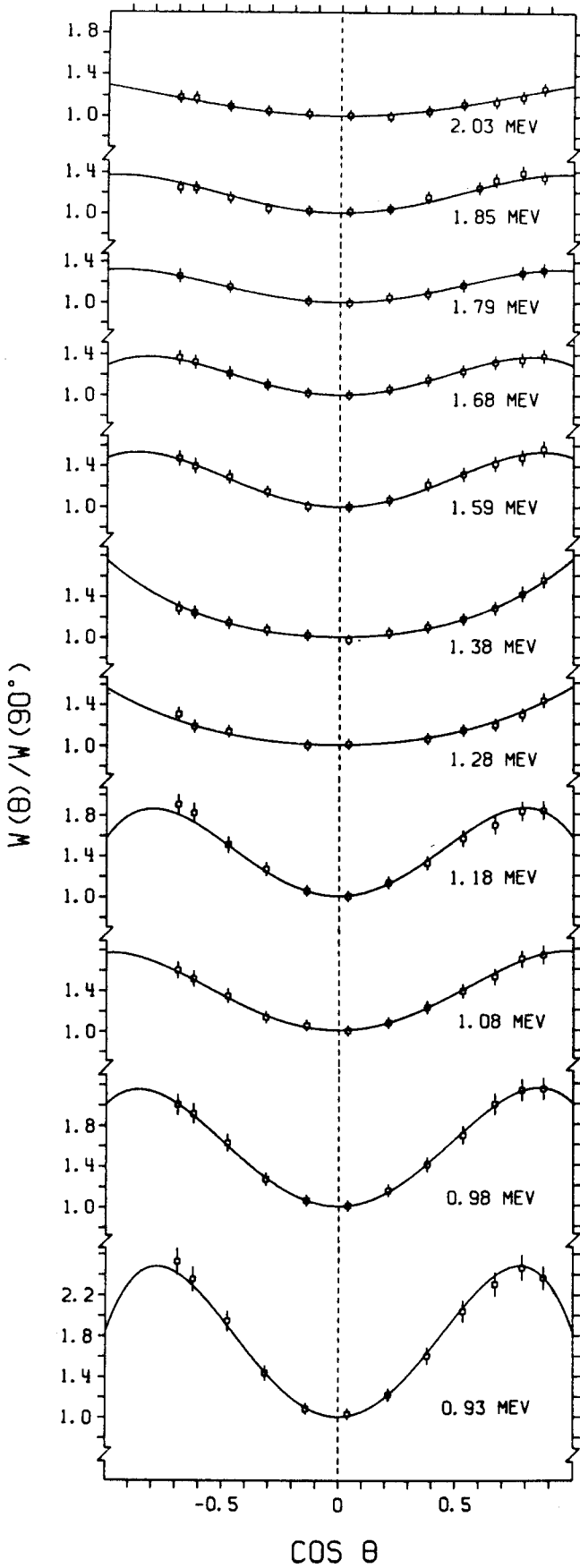


Figure 2

Figure 3



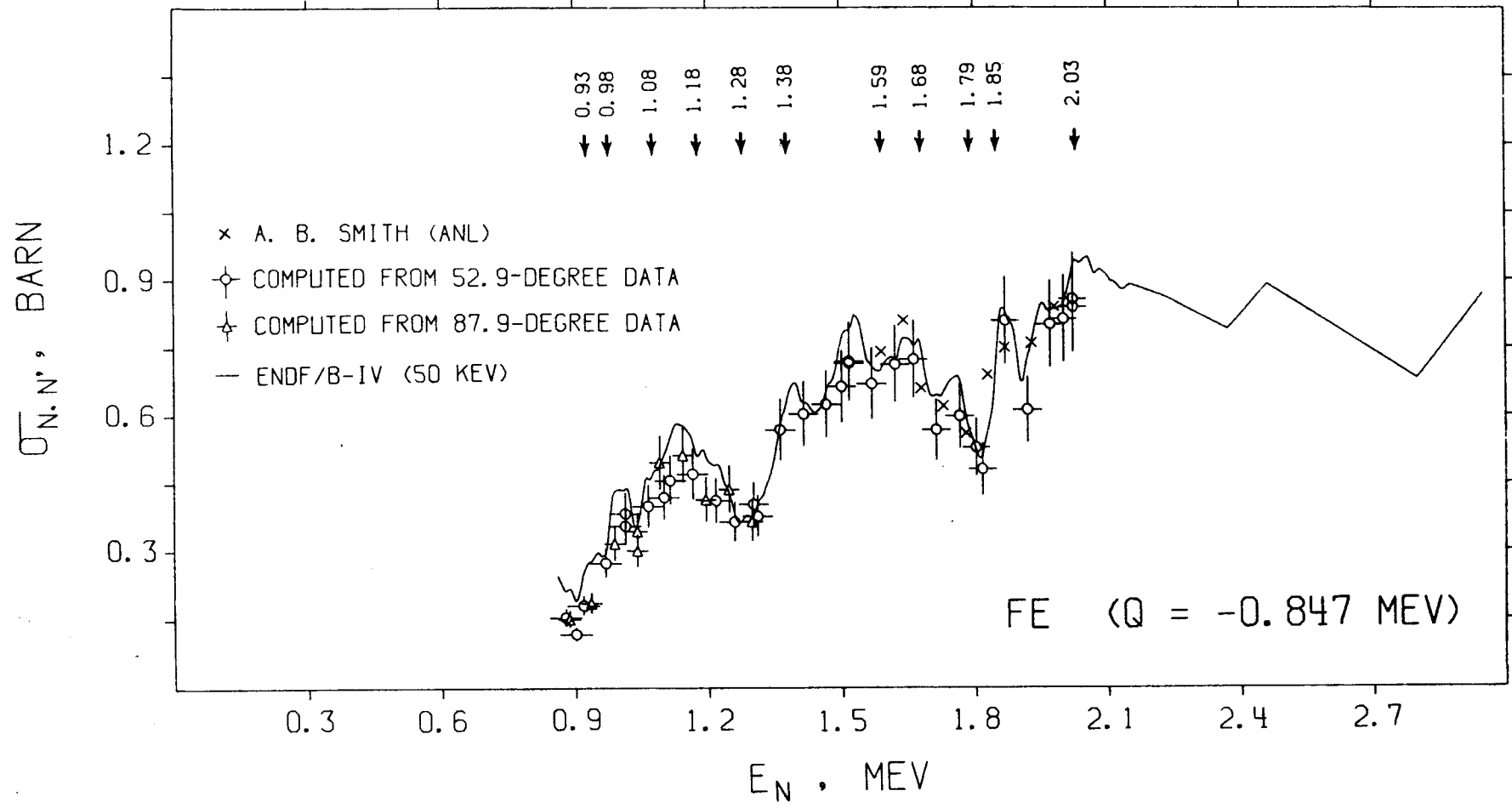


Figure 4

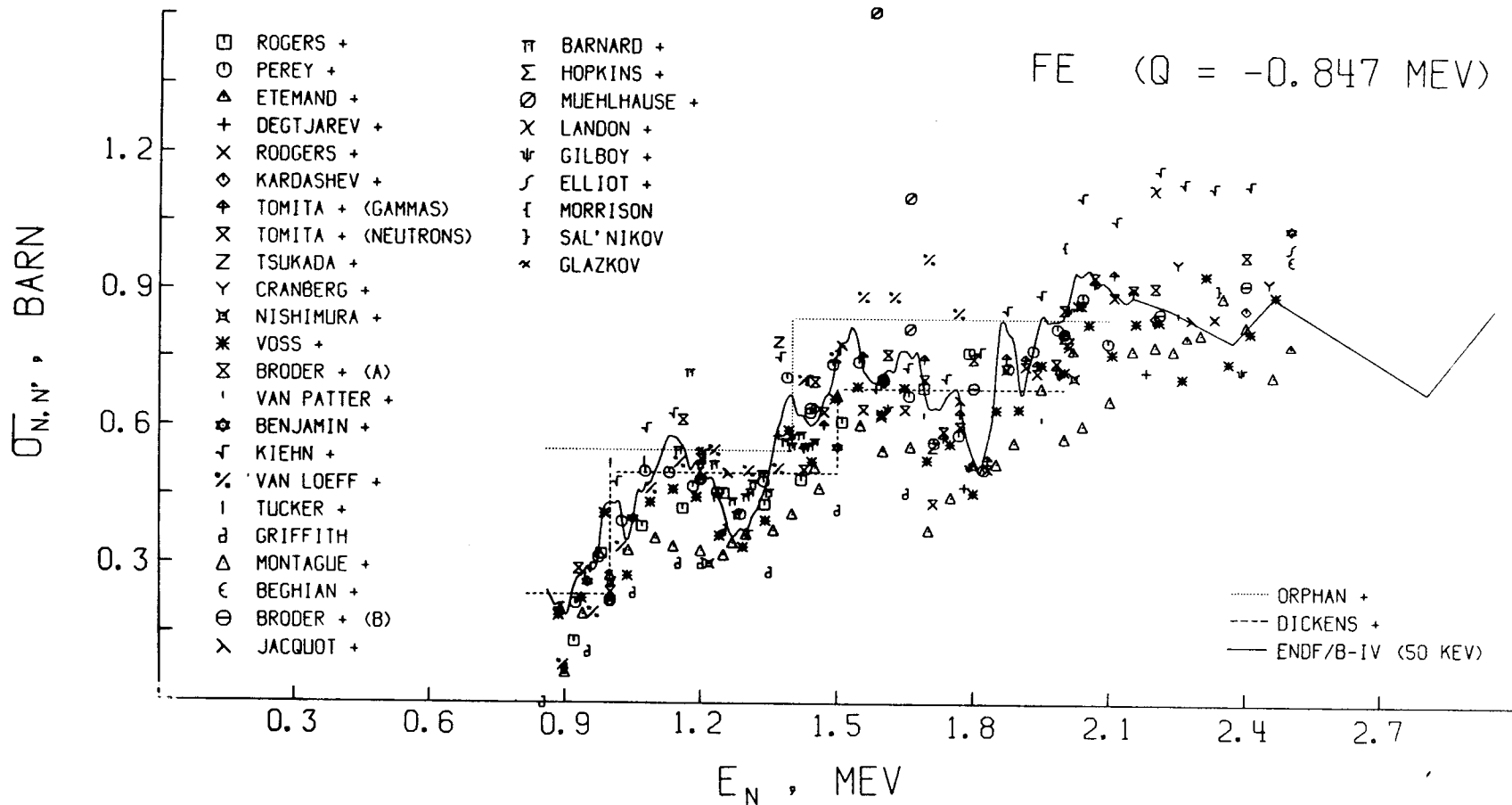


Figure 5

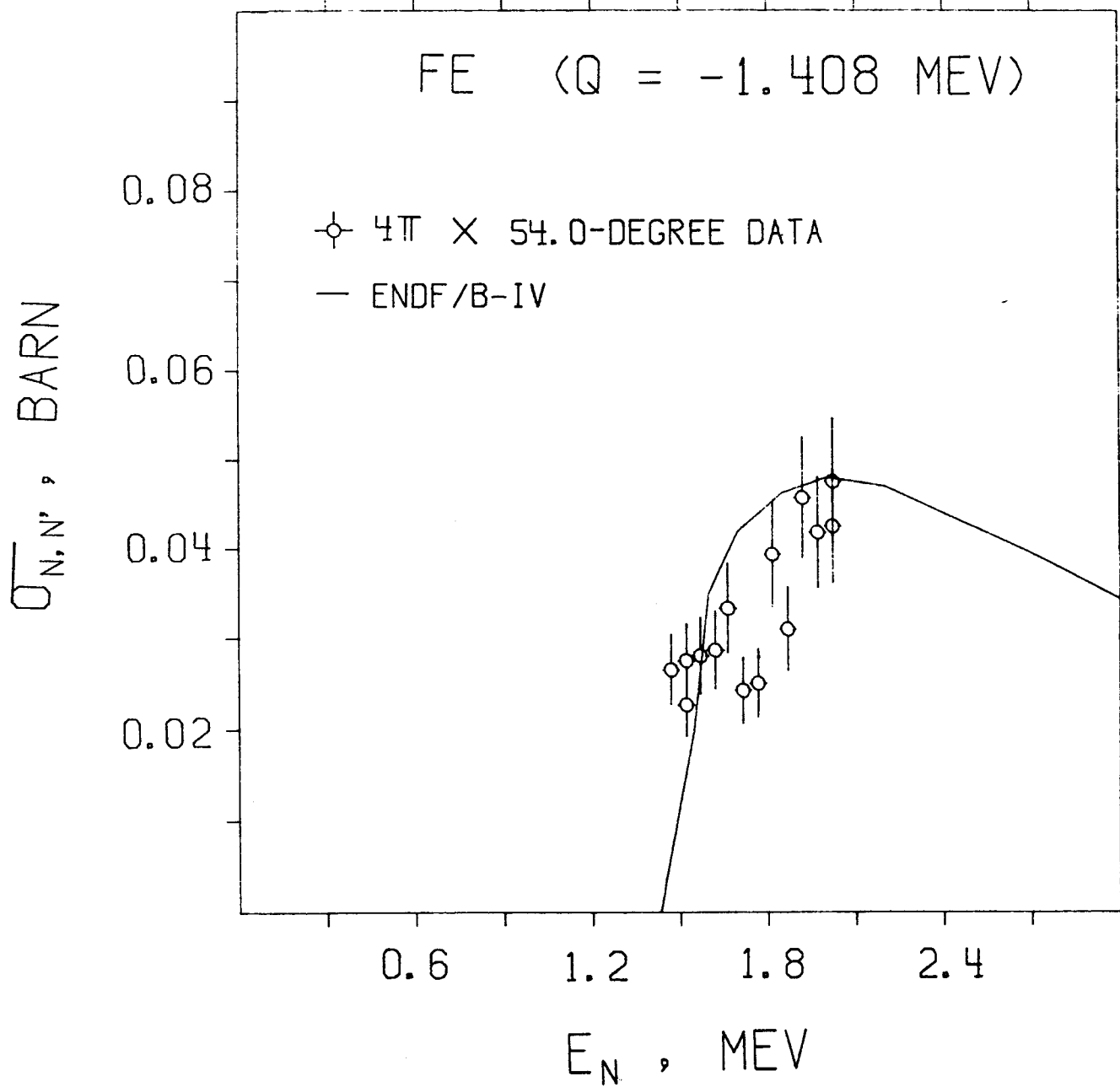


Figure 6

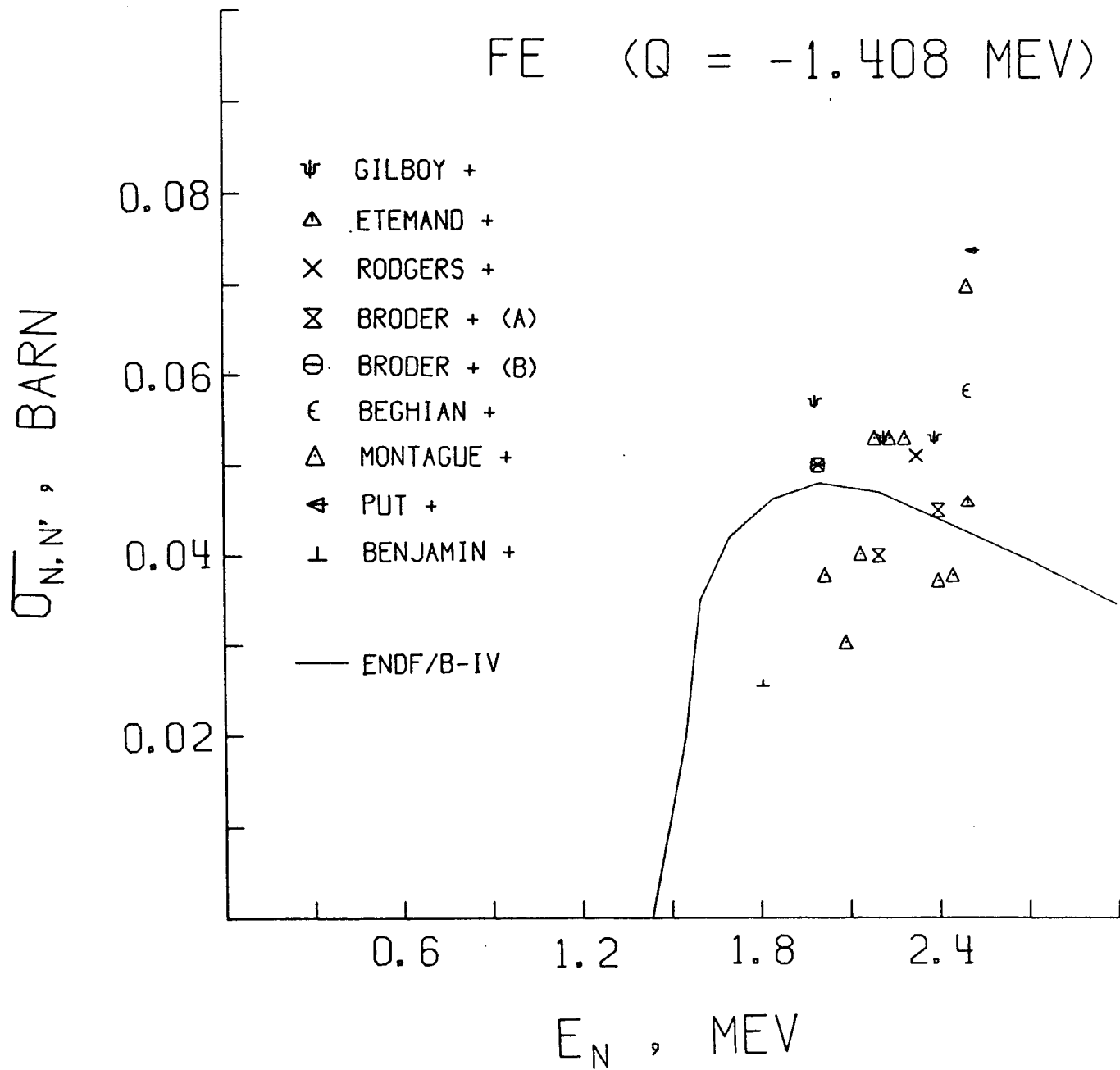


Figure 7